International Journal of Heat and Mass Transfer 54 (2011) 4410–4428

Contents lists available at ScienceDirect

International Journal of Heat and Mass Transfer

journal homepage: www.elsevier.com/locate/ijhmt

A critical synthesis of thermophysical characteristics of nanofluids

Khalil Khanafer [a,b], Kambiz Vafai [c,*]

[a] Vascular Mechanics Laboratory, Department of Biomedical Engineering, University of Michigan, Ann Arbor, MI 48109, USA
[b] Vascular Mechanics Laboratory, Section of Vascular Surgery, University of Michigan, Ann Arbor, MI 48109, USA
[c] Mechanical Engineering Department, University of California, Riverside, CA 92521, USA

ARTICLE INFO

Article history:
Received 18 March 2011
Received in revised form 18 April 2011
Accepted 18 April 2011
Available online 1 June 2011

Keywords:
Boiling
Free and forced convection
Nanofluids
Review
Surface tension
Thermophyscical properties

ABSTRACT

A critical synthesis of the variants within the thermophysical properties of nanofluids is presented in this work. The experimental results for the effective thermal conductivity and viscosity reported by several authors are in disagreement. Theoretical and experimental studies are essential to clarify the discrepancies in the results and in proper understanding of heat transfer enhancement characteristics of nanofluids. At room temperature, it is illustrated that the results of the effective thermal conductivity and viscosity of nanofluids can be estimated using the classical equations at low volume fractions. However, the classical models fail to estimate the effective thermal conductivity and viscosity of nanofluids at various temperatures. This study shows that it is not clear which analytical model should be used to describe the thermal conductivity of nanofluids. Additional theoretical and experimental research studies are required to clarify the mechanisms responsible for heat transfer enhancement in nanofluids. Correlations for effective thermal conductivity and viscosity are synthesized and developed in this study in terms of pertinent physical parameters based on the reported experimental data.

1. Introduction

Recent advances in nanotechnology have led to the development of a new, innovative class of heat transfer fluids (nanofluids) created by dispersing nanoparticles (10–50 nm) in traditional heat transfer fluids [1]. Nanofluids appear to have the potential to significantly increase heat transfer rates in a variety of areas such as industrial cooling applications, nuclear reactors, transportation industry (automobiles, trucks, and airplanes), micro-electromechanical systems (MEMS), electronics and instrumentation, and biomedical applications (nano-drug delivery, cancer therapeutics, cryopreservation) [2]. Possible improved thermal conductivity translates into higher energy efficiency, better performance, and lower operating costs.

A large number of research work related to the heat transfer enhancement using nanofluids both experimentally and theoretically was conducted by a number of investigators [1–15]. Although various studies have shown that nanofluids illustrate higher heat transfer enhancement than those of base fluids, contradictory results on nanofluids behavior were also reported. For example, Pak and Cho [16] demonstrated that the Nusselt number for Al_2O_3–water and TiO_2–water nanofluids increased with increasing volume fraction as well as the Reynolds number. However, the convective heat transfer coefficient for nanofluids at a volume fraction of 3% was found to be 12% smaller than that of pure water when considering a constant average velocity [16]. Yang et al. [17] reported a similar conclusion for graphite nanofluids in the laminar flow regime. On the contrary, many other researchers have reported heat transfer enhancement using nanofluids [6,11,15,18–22]. For instance, Xuan and Li [15] conducted an experimental study to investigate convective heat transfer and flow features of nanofluids. Their results show that convective heat transfer coefficient of the nanofluid increased with the flow velocity as well as the volume fraction of nanoparticles and it was larger than that of the base water under the same flow velocity. Das et al. [22] had shown experimentally that the thermal conductivity of nanofluid increases with an increase in temperature. They observed that a 2 to 4-fold increase in the thermal conductivity can be achieved over the temperature range of 21–52 °C.

In contrast to research investigations related to forced convective heat transfer using nanofluids, few studies are found in the literature on the use of nanofluids in natural convective heat transfer. Khanafer et al. [6] conducted a numerical study to determine natural convection heat transfer of nanofluids in an enclosure under various physical constraints. Their results illustrated that the average Nusselt number increases with an increase in the particle volume fraction for different Grashof numbers. Kim et al. [23] proposed a factor which described the effect of nanoparticle addition on the convective instability and heat transfer characteristics of a base fluid. The new factor included the effect of the ratio of the thermal conductivity of nanoparticles to that of the base fluid,

* Corresponding author. Tel.: +1 951 827 2135; fax: +1 951 827 2899.
E-mail address: vafai@engr.ucr.edu (K. Vafai).

0017-9310/$ - see front matter © 2011 Elsevier Ltd. All rights reserved.
doi:10.1016/j.ijheatmasstransfer.2011.04.048

Nomenclature

c_{eff}	heat capacity of nanofluids
c_f	heat capacity of the base fluid
c_p	heat capacity of nanoparticles
d_p	nanoparticles diameter
h	inter-particle spacing
k	thermal conductivity
k_B	Stefan–Boltzmann constant
k_{eff}	thermal conductivity of nanofluids
k_H	Huggins coefficient
k_{layer}	thermal conductivity of the nano-layer
m	mass
n	empirical shape factor
Pr	Prandtl number
Re	Reynolds number
t	thickness of the nano-layer
T	temperature
V	volume

Greek symbols

β_{eff}	thermal expansion coefficient of nanofluids
β_f	thermal expansion coefficient of the base fluid
β_p	thermal expansion coefficient of nanoparticle
ρ	density
ρ_{eff}	density of nanofluids
ψ	particle sphericity
ϕ_p	volume fraction of nanoparticles
$\phi_{p,\max}$	maximum volume fraction of nanoparticles
μ_{eff}	dynamic viscosity of nanofluids
μ_f	dynamic viscosity of the base fluid
$\mu_{Brownian}$	dynamic viscosity due to Brownian motion

Subscripts

f	fluid
p	nanoparticle

shape factor of the nanoparticles, volume fraction of nanoparticles, and the heat capacity ratio. Their results indicate that the heat transfer coefficients in the presence of nanofluids increases with an increase in the volume fraction of nanoparticles. Convective heat transfer enhancement using nanofluids was also observed experimentally by Nanna et al. [24] and Nanna and Routhu [25].

On the other hand, Putra et al. [13] found experimentally that the presence of nanoparticles (Al_2O_3 and CuO) in water based nanofluids inside a horizontal cylinder decreased natural convective heat transfer coefficient with an increase in the volume fraction of nanoparticles, particle density as well as the aspect ratio of the cylinder. Ding et al. [26] have also reported experimentally that natural convective heat transfer coefficient decreases systematically with an increase in nanoparticle concentration, and the deterioration was partially attributed to the higher viscosity of nanofluids. Chang et al. [27] performed natural convection experiments with Al_2O_3 microparticle ($\sim$250 nm) aqueous suspensions in thin enclosures. Their results seem to indicate that the particles have a negligible effect on the Nusselt number values for a vertical enclosure. However, for horizontal enclosure, there was a decrease in Nusselt number compared to presence of pure water at lower Rayleigh numbers and higher particle concentrations. The authors attributed this anomalous behavior to sedimentation.

Ho et al. [28] had experimentally investigated natural convection heat transfer of a nanofluid in a vertical enclosure for different particle sizes and various volume fractions of nanoparticles (Al_2O_3) ranging from 0.1% to 4% and Rayleigh number variations in the range of 10^5–10^8. Systematic heat transfer degradation was observed in their measurements for nanofluids containing nanoparticles with volume fractions greater than 2% over the entire range of Rayleigh numbers. However, heat transfer enhancement around 18% compared with pure water was exhibited for nanofluid containing lower nanoparticle concentrations of 0.1% at high Rayleigh numbers.

Currently, there are no reliable theoretical models to determine the anomalous thermal conductivity of nanofluids. Many researchers have based the thermal conductivity of nanofluids on thermal conductivities of fluid and nanoparticles, shape and surface area of nanoparticles, volume fraction, and temperature [29]. Keblinski et al. [30] and Eastman et al. [31] proposed four main mechanisms for thermal conductivity enhancement of nanofluids. These include Brownian motion of nanoparticles, molecular-level layering of the liquid at the liquid/particle interface, heat transport within the nanoparticles and the effects of nanoparticle clustering. They had reasoned that the effect of Brownian motion can be neglected due to the greater input of the thermal diffusion as compared to the Brownian diffusion. Evans et al. [32] had also demonstrated that the hydrodynamics effects associated with Brownian motion have a minor effect on the thermal conductivity of the nanofluid using the molecular dynamics simulations and the simple kinetic theory.

The effect of the solid/liquid interfacial layer on the thermal conductivity enhancement of nanofluids was studied theoretically by many researchers [33–38]. For example, Yu and Choi [33,34] proposed a theoretical model for the effect of a solid/liquid interface based on the Hamilton–Crosser model for suspensions of nonspherical particles. They attempt to demonstrate that the solid/liquid interfacial layers plays an important role in augmenting the thermal conductivity of nanofluids through the use of their Hamilton–Crosser model. However, their proposed model was unable to predict the nonlinear behavior of the nanofluid thermal conductivity. Considering the interface effect between the nanoparticles and base fluid, Xue [36] developed a theoretical model for the effective thermal conductivity for nanofluids based on Maxwell theory and average polarization theory. Xue [36] postulated that the developed model can interpret the anomalous enhancement of the effective thermal conductivity of the nanofluid. Other theoretical studies in the literature indicate additional conflicting results. Based on molecular dynamic simulations and simple liquid-solid interfaces, Xue et al. [38] illustrated that the layering of the liquid atoms at the liquid–solid interface does not have any considerable effect on thermal transport properties.

One can notice from the earlier cited information that neither Brownian motion nor interfacial liquid layering can be a dominant mechanism and that the findings from experimental and analytical investigations on the heat transfer enhancement using nanofluids are in disagreement for both natural and forced convection. Hence, further theoretical and experimental research are essential in order to explain the basis for possible heat transfer enhancement when using nanofluids. Although many possible mechanisms were proposed in the literature, there is no robust description of the anomalous behavior of nanofluids including higher thermal conductivity and viscosity. The thermal conductivity and viscosity data of nanofluids are still contradictory in various research publications. As such, it is still unclear as to what are the best models to use for the thermal conductivity and viscosity of nanofluids. Therefore, the aim of this study is to analyze the variants within the thermophysical characteristics of nanofluids especially with respect to the

thermal conductivity and viscosity models and propose possible physical reasons for the deviations between experimental and analytical studies.

1.1. Analytical models for physical properties of nanofluids

1.1.1. Density

The density of nanofluid is based on the physical principle of the mixture rule. As such it can be represented as:

$$\rho_{eff} = \left(\frac{m}{V}\right)_{eff} = \frac{m_f + m_p}{V_f + V_p} = \frac{\rho_f V_f + \rho_p V_p}{V_f + V_p} = (1-\phi_p)\rho_f + \phi_p \rho_p, \quad (1)$$

where f and p refer to the fluid and nanoparticle respectively and $\phi_p = \frac{V_p}{V_f + V_p}$ is the volume fraction of the nanoparticles. To examine the validity of Eq. (1), Pak and Cho [16] and Ho et al. [28] conducted experimental studies to measure the density of Al_2O_3–water nanofluids at room temperature as depicted in Fig. 1a. Fig. 1a shows an excellent agreement between the experimental results and the predictions using Eq. (1).

The physical properties at different temperatures are very important for engineering calculations. Ho et al. [28] measured the density of Al_2O_3–water nanofluid at different temperatures and nanoparticle volume fractions. In the present work, a correlation for the density of Al_2O_3–water nanofluid using the experimental data of Ho et al. [28] as a function of temperature and volume fraction of nanoparticles has been developed. The present developed correlation can be expressed as:

$$\rho_{eff} = 1001.064 + 2738.6191\phi_p - 0.2095T; \quad 0 \leqslant \phi_p \leqslant 0.04, 5 \leqslant T(^{\circ}\mathrm{C}) \leqslant 40. \quad (2)$$

The R^2 of the regression is 99.97% and the maximum relative error is 0.22%. It is clear from Fig. 1b that the current regression (Eq. (2)) is in excellent agreement with the measurements of Ho et al. [28]. In addition, Fig. 1b shows that the rate of decrease of the effective density of Al_2O_3–water nanofluid with increasing temper-

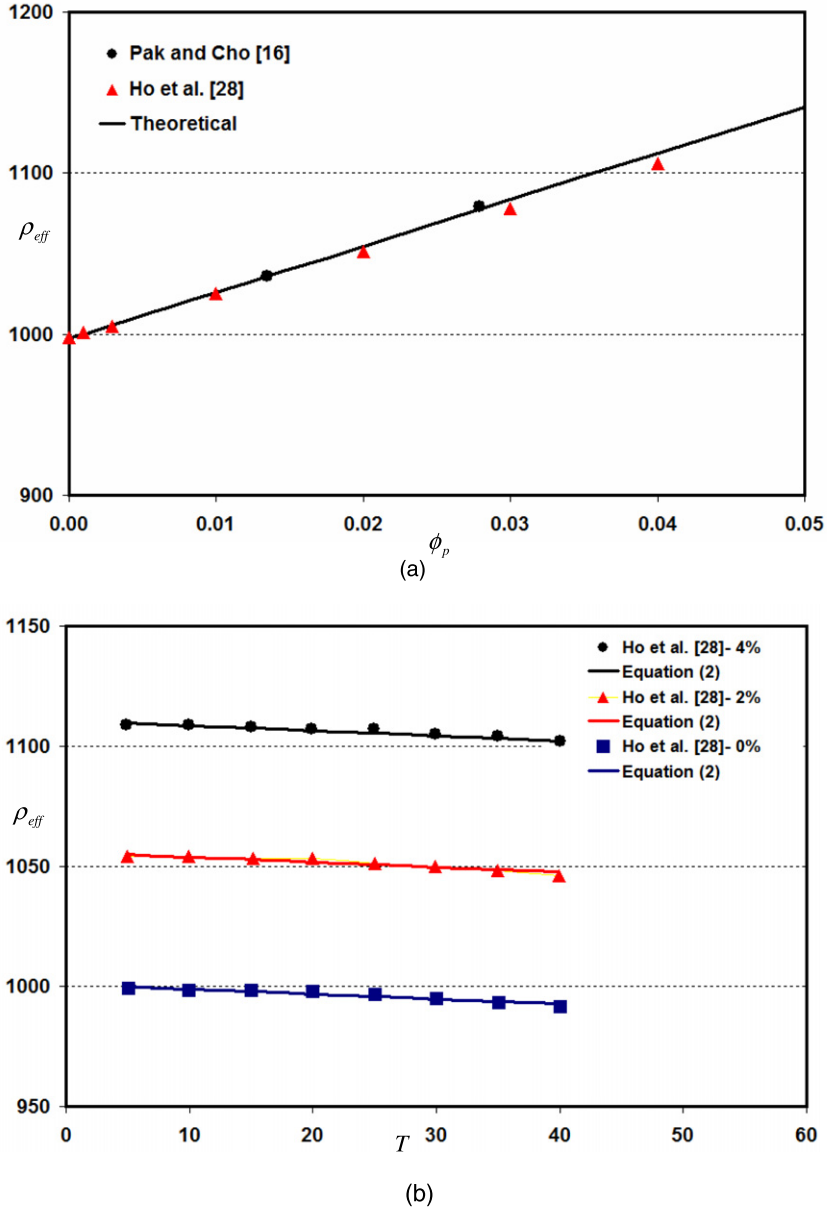

Fig. 1. Effect of the volume fraction on the density of the Al_2O_3–water nanofluid (a) room temperature; (b) various temperatures.

ature is insignificant. This is due to the fact that the density of the Al_2O_3 nanoparticles is even less sensitive to the temperature when compared to the density of water.

2. Heat capacity of nanofluids

The specific heat of nanofluid can be determined by assuming thermal equilibrium between the nanoparticles and the base fluid phase as follows:

$$(\rho c)_{eff} = \rho_{eff}\left(\frac{Q}{m\Delta T}\right)_{eff} = \rho_{eff}\frac{Q_f + Q_p}{(m_f + m_p)\Delta T} = \frac{(mc)_f\Delta T + (mc)_p\Delta T}{(m_f + m_p)\Delta T} \rightarrow (\rho c)_{eff} = \rho_{eff}\frac{(\rho c)_f V_f + (\rho c)_p V_p}{\rho_f V_f + \rho_p V_p} \Rightarrow c_{eff} = \frac{(1-\phi_p)\rho_f c_f + \phi_p \rho_p c_p}{\rho_{eff}} \quad (3)$$

where ρ_p is the density of the nanoparticle, ρ_f is the density of the base fluid, ρ_{eff} is the density of the nanofluid, and c_p and c_f are the heat capacities of the nanoparticle and the base fluid, respectively. However, some authors [16,22,39–41] prefer to use a simpler expression given as:

$$c_{eff} = (1-\phi_p)c_f + \phi_p c_p. \quad (4)$$

Fig. 2 shows a comparison of the specific heat of Al_2O_3–water nanofluid at room temperature using both equations with the experimental data of Zhou and Ni [42] for various volume fractions ($\phi_p = 0$—21.7%). This figure shows that the specific heat of the nanofluid based on the models given in Eqs. (3) and (4) decreases with an increase in the volume fraction of nanoparticles. The experimental results were compared with the predictions obtained from the models given in Eqs. (3) and (4) as shown in Fig. 2. Fig. 2 shows that model I compares very well with the experimental data of Zhou and Ni [42].

3. Thermal expansion coefficient of nanofluids

The thermal expansion coefficient of nanofluids can be estimated utilizing the volume fraction of the nanoparticles on a weight basis as follows [6]:

$$\beta_{eff} = \frac{(1-\phi_p)(\rho\beta)_f + \phi_p(\rho\beta)_p}{\rho_{eff}}, \quad (4)$$

where β_f and β_p are the thermal expansion coefficients of the base fluid and the nanoparticle, respectively. A simpler model for the thermal expansion coefficient of the nanofluid is suggested as [43,44]:

$$\beta_{eff} = (1-\phi_p)\beta_f + \phi_p\beta_p. \quad (5)$$

To the best of our knowledge, there is one experimental measurement of the volumetric expansion coefficient of nanoparticles that has been reported in the literature [28]. Ho et al. [28] conducted an experimental study to determine the thermal expansion of Al_2O_3–water nanofluid at various volume fractions of nanoparticles. For water, β_f varies from $1.5\times10^{-4}\,^{\circ}C^{-1}$ to $6.2\times10^{-4}\,^{\circ}C^{-1}$ over a temperature range of $15\,^{\circ}C \leqslant T \leqslant 80\,^{\circ}C$, which is two orders of magnitude higher than β_p. The values of the thermal expansion of Al_2O_3–water nanofluid predicted by Eqs. (4) and (5) were compared with the experimental data of Ho et al. [28] at a temperature of 26 °C. Fig. 3a shows that neither Eq. (4) nor Eq. (5) can be used to properly estimate the thermal expansion of nanofluid as compared to the experimental data of Ho et al. [28].

Ho et al. [28] also studied the effect of temperature and volume fraction of nanoparticles on the thermal expansion coefficient of Al_2O_3–water nanofluid. A correlation for the thermal expansion coefficient of Al_2O_3–water nanofluid as a function of temperature and volume fraction of nanoparticles based on the data presented in Ho et al. [28] has been developed in the current work. This correlation can be presented as:

$$\beta_{eff} = \left(-0.479\phi_p + 9.3158\times10^{-3}T - \frac{4.7211}{T^2}\right)\times10^{-3}; \quad 0 \leqslant \phi_p \leqslant 0.04, \quad 10\,^{\circ}C \leqslant T \leqslant 40\,^{\circ}C \quad (6)$$

The R^2 of the above correlation is 99%. The validity of this correlation (Eq. (6)) is depicted in Fig. 3b.

4. Effective viscosity of nanofluids

4.1. Analytical studies

Different models of viscosity have been used by researchers to model the effective viscosity of nanofluid as a function of volume fraction. Einstein [45] determined the effective viscosity of a suspension of spherical solids as a function of volume fraction (volume concentration lower than 5%) using the phenomenological hydrodynamic equations. This equation was expressed by:

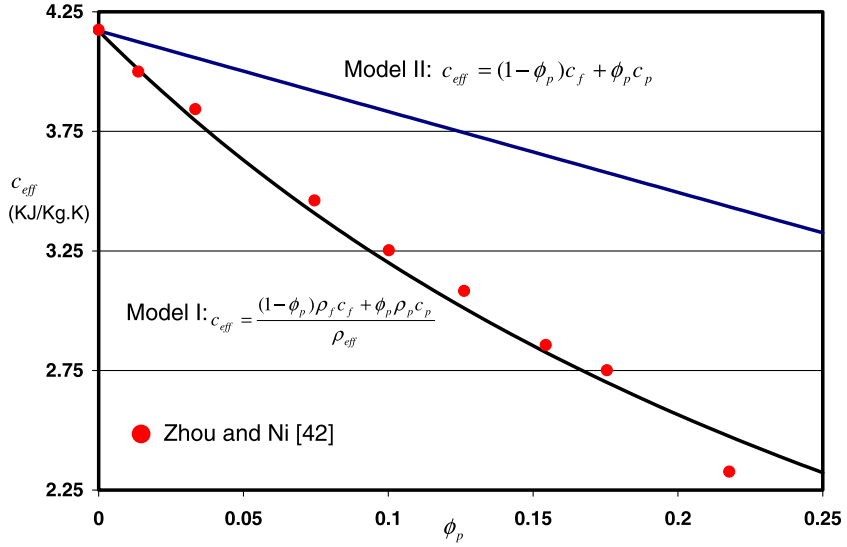

Fig. 2. Comparison of the heat capacity of Al_2O_3–water nanofluid obtained by models I and II given in Eqs. (3) and (4) and the experimental data of Zhou and Ni [42].

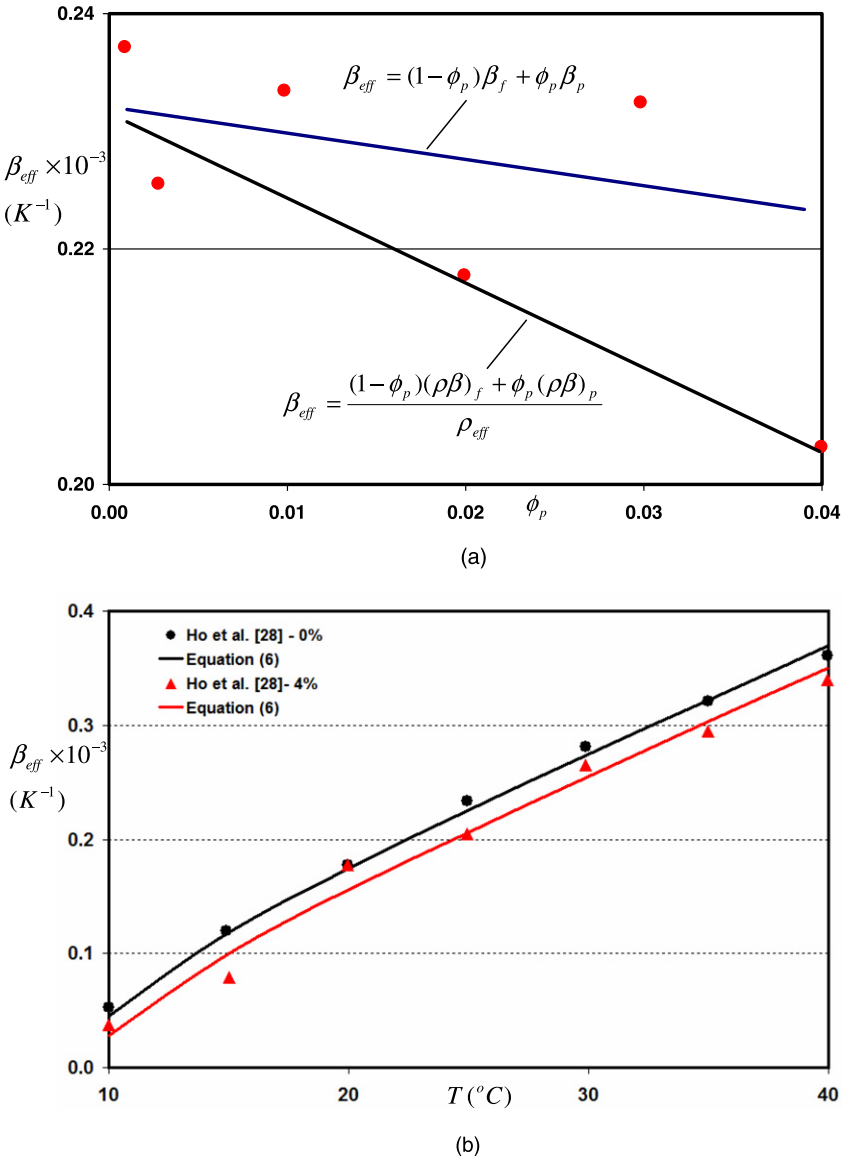

Fig. 3. Effect of the volume fraction and temperature on the thermal expansion coefficient of Al_2O_3–water nanofluid (a) effect of volume fraction as displayed by Eqs. (4) and (5) at room temperature; (b) temperature effect as displayed by a comparison between Eq. (6) and experimental data of Ho et al. [28].

$$\mu_{eff} = (1 + 2.5\phi_p)\mu_f. \tag{7}$$

Since Einstein's analysis of the viscosity of a dilute suspension of rigid spheres in a viscous liquid, several equations have been developed in an effort to extend Einstein's formula to suspensions of higher concentrations, including the effect of non-spherical particle concentrations [46–50]. For example, Brinkman [46] presented a viscosity correlation that extended Einstein's equation to concentrated suspensions:

$$\mu_{eff} = \frac{1}{(1-\phi_p)^{2.5}} = (1 + 2.5\phi_p + 4.375\phi_p^2 + \cdots)\mu_f. \tag{8}$$

The effect of Brownian motion on the effective viscosity in a suspension of rigid spherical particles was studied by Batchelor [47]. For isotropic structure of suspension, the effective viscosity was given by:

$$\mu_{eff} = \left(1 + 2.5\phi_p + 6.2\phi_p^2\right)\mu_f. \tag{9}$$

Lundgren [48] proposed the following equation under the form of a Taylor series in ϕ_p:

$$\mu_{eff} = \frac{1}{1-2.5\phi_p}\mu_f = \left(1 + 2.5\phi_p + 6.25\phi_p^2 + O(\phi_p^3)\right)\mu_f. \tag{10}$$

It is obvious that if the terms $O(\phi_p^2)$ and higher are neglected, the above correlation reduces to that of Einstein. Table 1 summarizes the most common analytical expressions for the viscosity of nanofluids as a function of the volume fraction of the nanoparticles.

4.2. Experimental studies

Compared with the experimental studies on thermal conductivity of nanofluids, there are limited rheological studies reported in the literature [16,55–63]. Models of the effective viscosity of nanofluids based on the experimental data are limited to certain nanofluids. Masuda et al. [56] were the first to measure the viscosity of several water-based nanofluids for temperatures ranging from room condition to 67 °C. Wang et al. [55] obtained, using three different preparation methods, some data for the dynamic viscosity of Al_2O_3–water and Al_2O_3–ethylene glycol mixtures at various temperatures.

Table 1
Summarizes a significant number of models found in the literature.

Models	Effective viscosity	Physical model	Remarks
Einstein [45]	$\mu_{eff} = (1 + 2.5\phi_p)\mu_f$	– Based on the phenomenological hydrodynamic equations – Considered a suspension containing n solute particles in a total volume V	– Infinitely dilute suspension of spheres (no interaction between the spheres) – Valid for relatively low particle volume fraction ($\phi_p \leqslant 2\%$)
Brinkman [46]	$\mu_{eff} = \frac{1}{(1-\phi_p)^{2.5}} = (1 + 2.5\phi_p + 4.375\phi_p^2 + \ldots)\mu_f$	– Based on Einstein model – Derived by considering the effect of the addition of one solute-molecule to an existing solution	– Spherical particles – Valid for high moderate particle concentrations – Used Einstein's factor: $(1 + 2.5\phi_p)$
Batchelor [47]	$\mu_{eff} = (1 + \eta\phi_p + k_H\phi_p^2)\mu_f = (1 + 2.5\phi_p + 6.2\phi_p^2)\mu_f$	– Based on reciprocal theorem in Stokes flow problem to obtain an expression for the bulk stress due to the thermodynamic forces – Incorporated both effects: hydrodynamic effects and Brownian motion	– Rigid and Spherical particles – Brownian motion – Isotropic structure – Huggins coefficient: $k_H = 6.2$ (5.2 from hydrodynamic effects and 1.0 from Brownian motion)
Lundgren [48]	$\mu_{eff} = \frac{1}{1-2.5\phi_p}\mu_f = (1 + 2.5\phi_p + 6.25\phi_p^2 + \ldots)\mu_f$	– Based on a Taylor series expansion in terms of ϕ_p	– Dilute concentration of spheres – Random bed of spheres
Graham [49]	$\mu_{eff} = (1 + 2.5\phi_p)\mu_f + \left[\frac{4.5}{(h/r_p)\cdot(2+h/r_p)\cdot(1+h/r_p)^2}\right]\mu_f$	– A cell theory was used to derive the dependence of the zero-shear-rate viscosity on volume concentration for a suspension of uniform, solid, neutrally buoyant spheres	– Agrees well with Einstein's for small ϕ_p – r_p is the particle radius and h is the inter-particle spacing
Simha [50]	$\mu_{eff} = \left[1 + 2.5\phi_p + \left(\frac{125}{64\phi_{p\max}}\right)\phi_p^2 + \ldots\right]\mu_f$	– Based on Cage model of liquids and solutions	– Spherical particles
Mooney [51]	$\mu_{eff} = \exp\left(\frac{2.5\phi_p}{1-k\phi_p}\right)\mu_f = \{1 + 2.5\phi_p + [3.125 + (2.5k)]\phi_p^2 + \ldots\}\mu_f 1.35 < k < 1.91$	– Einstein's viscosity equation for an infinitely dilute suspension of spheres was extended to apply to a suspension of finite concentration – Based on first-order interaction between particles (crowding effect)	– Rigid spherical spheres – Monodisperse suspension of finite concentration – Not valid at high concentrations – Considered the volume fraction of a suspension to be divided into two portions
Eilers [52]	$\mu_{eff} = \mu_f[1 + \frac{1.25\phi_p}{1-\phi_p/0.78}] = (1 + 2.5\phi_p + 4.75\phi_p^2 + \ldots)\mu_f$	– Based on experimental data	– Suspensions of bitumen spheres – Curve fitting of the experimental data
Saito [53]	$\mu_{eff} = \left(1 + \frac{2.5}{1-\phi_p}\phi_p\right)\mu_f = (1 + 2.5\phi_p + 2.5\phi_p^2 + \ldots)\mu_f$	– Developed based on a theory for spherical solute-molecules in which a single solute-molecule is placed in the field of flow, obtained by averaging over all the possible positions of a second solute-molecule	– Spherical rigid particles – Brownian motion – Very small particles
Frankel and Acrivos [54]	$\mu_{eff} = \left(\frac{9}{8}\frac{(\phi_p/\phi_{p\max})^{1/3}}{1-(\phi_p/\phi_{p\max})^{1/3}}\right)\mu_f$	– An asymptotic technique was used to derive the functional dependence of effective viscosity on concentration for a suspension of uniform solid spheres, in the limit as concentration approaches its maximum value	– Uniform solid particles

Because the formulas such as the one proposed by Einstein [45] and later improved by Brinkman [46] and Batchelor [47] underestimate the viscosity of the nanofluids when compared to the measured data, Maiga et al. [57,58] performed a least-square curve fitting of some experimental data of Wang et al. [55] including Al_2O_3 in water and Al_2O_3 in ethylene glycol. Table 2 illustrates a summary of the viscosity models at room temperature based on the experimental data available in the literature. Moreover, Fig. 4 shows a comparison of the relative dynamic viscosity of Al_2O_3–water nanofluid from various sources at room temperature. This figure shows that Brinkman model [46], which was derived for two-phase mixture, is to some extent sufficient to estimate the viscosity for relatively low volume fraction of particles (i.e., $\phi_p \leqslant 2\%$). However, it considerably underestimates the nanofluid viscosity when compared to experimental data at high particle concentrations. The differences in the relative viscosity among the experimental data as shown in Fig. 4 may be due to the difference in the size of the particle clusters, dispersion techniques, and the methods of measurements. This clearly shows the disagreement between the researchers in measuring the viscosity of nanofluids.

4.3. Effect of temperature on the dynamic viscosity of nanofluids

It should be noted that all the above mentioned correlations were developed to relate viscosity as a function of volume fraction only; without any temperature dependence considerations. It should be mentioned that there exists a few studies in the literature associated with the effect of temperature on the viscosity of nanofluids. For example, Nguyen et al. [60] investigated experimentally the influence of the temperature on the dynamic viscosities of two particular water-based nanofluids, namely Al_2O_3–water ($d_p = 47$ nm, 36 nm) and CuO–water ($d_p = 29$ nm) mixtures. The following formulas were proposed by Nguyen et al. [60] for computing the dynamic viscosity for all three nanofluids tested and particle concentrations of 1% and 4%, respectively:

$$\mu_{eff} = (1.125 - 0.0007 \times T)\mu_f; \quad \phi_p = 1\%, \tag{11}$$

$$\mu_{eff} = \left(2.1275 - 0.0215 \times T + 0.0002 \times T^2\right)\mu_f; \quad \phi_p = 4\%. \tag{12}$$

As can be seen from Eqs. (11) and (12), Nguyen et al. [60] did not explicitly express the dynamic viscosity as a function of temperature and volume fraction. Palm et al. [68] proposed equations for the dynamic viscosity (Pa s) by means of the polynomial curve fitting based on the data reported by Putra et al. [13]. The resulting equations as a function of temperature, expressed in Kelvin, are:

For Al_2O_3–water:

$$\mu_{eff} = 0.034 - 2 \times 10^{-4}T + 2.9 \times 10^{-7}T^2, \quad \phi_p = 1\%, \tag{13}$$

$$\mu_{eff} = 0.039 - 2.3 \times 10^{-4}T + 3.4 \times 10^{-7}T^2, \quad \phi_p = 4\%. \tag{14}$$

Table 2
Summary of viscosity models at room temperature based on experimental data.

Models	Effective viscosity (regression)	Remarks
Maiga et al. [57]	$\mu_{eff} = (1 + 7.3\phi_p + 123\phi_p^2)\mu_f$	– Least-square curve fitting of Wang et al. [55] data – Al_2O_3–water, d_p = 28 nm
Maiga et al. [57]	$\mu_{eff} = (1 - 0.19\phi_p + 306\phi_p^2)\mu_f$ $d_p = 28$ nm	– Least-square curve fitting of experimental data [55,56] – Al_2O_3–ethylene glycol
Present work	$\mu_{eff} = (1 + 0.164\phi_p + 302.34\phi_p^2)\mu_f$ $d_p = 28$ nm	– Least-square curve fitting of experimental data [55,56] – Al_2O_3–ethylene glycol
Buongiorno [67]	$\mu_{eff} = (1 + 39.11\phi_p + 533.9\phi_p^2)\mu_f$	– Curve fitting of Pak and Cho [16] data – Al_2O_3–water, d_p = 13 nm
Buongiorno [67]	$\mu_{eff} = (1 + 5.45\phi_p + 108.2\phi_p^2)\mu_f$	– Curve fitting of Pak and Cho [16] data – TiO_2–water, d_p = 27 nm
Present work	$\mu_{eff} = (1 + 23.09\phi_p + 1525.3\phi_p^2)\mu_f$ $0 \leqslant \phi_p \leqslant 0.04$	– Curve fitting of Pak and Cho [16] data – Al_2O_3–water, d_p = 13 nm
Present work	$\mu_{eff} = (1 + 3.544\phi_p + 169.46\phi_p^2)\mu_f$ $0 \leqslant \phi_p \leqslant 0.1$	– Curve fitting of Pak and Cho [16] data – TiO_2–water, d_p = 27 nm
Nguyen et al. [60]	$\mu_{eff} = \mu_f \times 0.904e^{0.148\phi_p}$; $d_p = 47$ nm, $\mu_{eff} = (1 + 0.025\phi_p + 0.015\phi_p^2)\mu_f$; $d_p = 36$ nm	– Curve fitting of the experimental data – Al_2O_3–water
Nguyen et al. [60]	$\mu_{eff} = (1.475 - 0.319\phi_p + 0.051\phi_p^2 + 0.009\phi_p^3)\mu_f$	– Curve fitting of the experimental data – CuO–water, d_p = 29 nm
Tseng and Lin [61]	$\mu_{eff} = 13.47\exp(35.98\phi_p)\mu_f; 0.05 \leqslant \phi_p \leqslant 0.12$	– TiO_2–water Shear rate = 100 s^{-1}

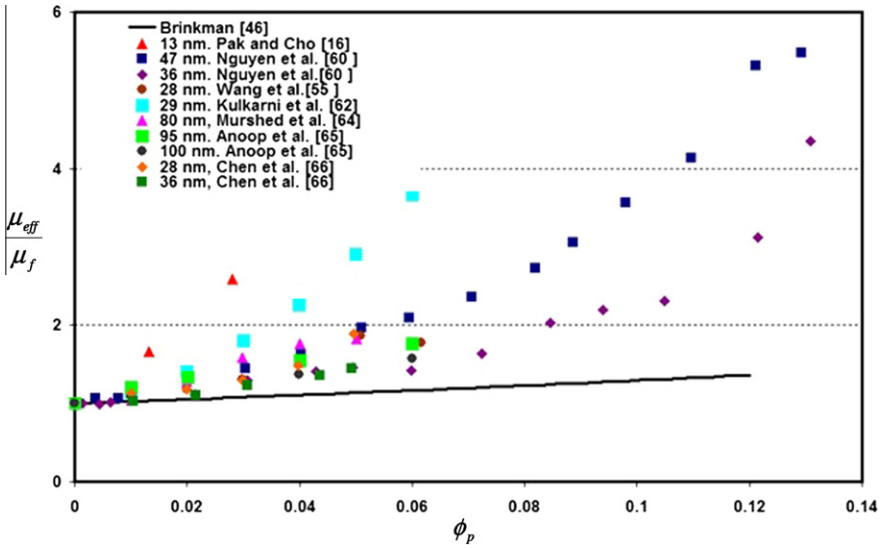

Fig. 4. Relative viscosity measurement as a function of the volume fraction, ϕ_p, at ambient temperature. (See above-mentioned references for further information.)

Tables 3 and 4 provide a summary of different models of the dynamic viscosity of nanofluids as a function of temperature and volume fraction of nanoparticles. In the present work, a general correlation (Eq. (15)) for the effective viscosity of Al_2O_3–water, one of the most commonly studied nanofluids, is developed using various experimental data found in the literature (Fig. 5a) as a function of volume fraction, nanoparticles diameter, and temperature as follows:

$$\mu_{eff} = -0.4491 + \frac{28.837}{T} + 0.574\phi_p - 0.1634\phi_p^2 + 23.053\frac{\phi_p^2}{T^2} + 0.0132\phi_p^3 - 2354.735\frac{\phi_p}{T^3} + 23.498\frac{\phi_p^2}{d_p^2} - 3.0185\frac{\phi_p^3}{d_p^2};$$
$$1\% \leqslant \phi_p \leqslant 9\%,\ 20 \leqslant T(^\circ\mathrm{C}) \leqslant 70,\ 13\ \mathrm{nm} \leqslant d_p \leqslant 131\ \mathrm{nm}. \quad (15)$$

The R^2 of the regression is 99%. The validity of the above correlation (Eq. (15)) is depicted in Fig. 5b. As can be seen in Fig. 5a, the viscosity of the nanofluid decreases with an increase in the temperature. Moreover, there is no agreement between researchers about the experimentally observed magnitude of the nanofluid's viscosity. Published results indicate a surprising range of variation of the results.

5. Thermal conductivity of nanofluids

A wide range of experimental and theoretical studies were conducted in the literature to model thermal conductivity of nanofluids. Published results illustrated neither agreement about the mechanisms for heat transfer enhancement nor a unified possible explanation regarding the rather large discrepancies in the results even for the same base fluid and nanoparticles size. Currently,

Table 3
Effect of temperature and volume fraction on the dynamic viscosity of nanofluids (Al_2O_3–water).

Reference	Model (regression)	Remarks
Present work	$\mu_{eff} = 0.444 - 0.254\phi_p + 0.0368\phi_p^2 + 26.333\frac{\phi_p}{T} - 59.311\frac{\phi_p^2}{T^2}$ $20 \leqslant T(oC) \leqslant 70; \phi_p = 1.34\%, 2.78\%$	– Curve fitting of Pak and Cho [16] data d_p = 13 nm – Units: mPa s
Palm et al. [68]	$\mu_{eff} = 0.034 - 2\times10^{-4}T(K) + 2.9\times10^{-7}T^2(K), \phi_p = 1\%$ $\mu_{eff} = 0.039 - 2.3\times10^{-4}T(K) + 3.4\times10^{-7}T^2(K), \phi_p = 4\%$	– Curve fitting of the experimental data Putra et al. [13] d_p = 131.2 nm – Units: Pa s
Nguyen et al. [60]	$\mu_{eff} = (1.125 - 0.0007\times T(^\circ\mathrm{C}))\mu_f\ ; \phi_p = 1\%$ $\mu_{eff} = (2.1275 - 0.0215\times T(^\circ\mathrm{C}) + 0.0002\times T^2(^\circ\mathrm{C}))\mu_f\ ; \phi_p = 4\%$	– Units: mPa s
Present work	$\mu_{eff} = -0.4892 + \frac{26.9036}{T} + 0.6837\phi_p + \frac{24.1141}{T^2} - 0.1785\phi_p^2 +$ $0.1818\frac{\phi_p}{T} + 27.015\frac{\phi_p^2}{T^2} + 0.0132\phi_p^3 - 2940.1775\frac{\phi_p}{T^3};$ $1\% \leqslant \phi_p \leqslant 9.4\%, 20 \leqslant T(^\circ\mathrm{C}) \leqslant 70$	– Curve fitting of Nguyen et al. [60] data d_p = 47 nm – Units: mPa s
Present work	$\mu_{eff} = -0.1011 + \frac{18.0162}{T} + 0.3619\phi_p + \frac{164.0837}{T^2} - 0.0966\phi_p^2 +$ $0.1609\frac{\phi_p}{T} + 22.4901\frac{\phi_p^2}{T^2} + 0.0078089\phi_p^3 - 2316.3754\frac{\phi_p}{T^3};$ $1\% \leqslant \phi_p \leqslant 9.1\%, 20 \leqslant T(^\circ\mathrm{C}) \leqslant 70$	– Curve fitting of Nguyen et al. [60] data d_p = 36 nm – Units: mPs s
Present work	$\mu_{eff} = -0.4491 + \frac{28.837}{T} + 0.574\phi_p - 0.1634\phi_p^2 + 23.053\frac{\phi_p^2}{T^2} +$ $0.0132\phi_p^3 - 2354.735\frac{\phi_p}{T^3} + 23..498\frac{\phi_p^2}{d_p^2} - 3.0185\frac{\phi_p^3}{d_p^2};$ $1\% \leqslant \phi_p \leqslant 9\%, 20 \leqslant T(^\circ\mathrm{C}) \leqslant 70, 13\ \mathrm{nm} \leqslant d_p \leqslant 131\ \mathrm{nm}$	– Curve fitting of various experimental data available in the literature [13,16,60,65] – Units: mPa s
Namburu et al. [70,71]	$Log(\mu_{eff}) = Ae^{-BT}$, in mm Pa s $A = -0.29956\phi_p^3 + 6.7388\phi_p^2 - 55.444\phi_p + 236.11$ $B = (-6.4745\phi_p^3 + 140.03\phi_p^2 - 1478.5\phi_p + 20341)/10^6$	– Experimental Al_2O_3–ethylene glycol and water mixture $1\% \leqslant \phi_p \leqslant 10\%, d_p = 53$ nm $238 < T < 323$ K

Table 4
Effect of temperature and volume fraction on the dynamic viscosity of nanofluids (TiO_2–water, CuO–water).

Models	Effective viscosity (regression)	Remarks
Duangthongsuk and Wongwises [69]	$\frac{\mu_{eff}}{\mu_f} = 1.0226 + 0.0477\phi_p - 0.0112\phi_p^2; T = 15\ ^\circ\mathrm{C}$ $\frac{\mu_{eff}}{\mu_f} = 1.013 + 0.092\phi_p - 0.015\phi_p^2; T = 25\ ^\circ\mathrm{C}$ $\frac{\mu_{eff}}{\mu_f} = 1.018 + 0.112\phi_p - 0.0177\phi_p^2; T = 35\ ^\circ\mathrm{C}$	– Experimental data – TiO_2–Water, $0.2 \leqslant \phi_p \leqslant 2\%$ – d_p = 21 nm
Present work	$\frac{\mu_{eff}}{\mu_f} = 1.0538 + 0.1448\phi_p - 3.363\times10^{-3}T - 0.0147\phi_p + 6.735\times10^{-5}T^2 -$ $1.337\frac{\phi_p}{T}\ 15\ ^\circ\mathrm{C} \leqslant T \leqslant 35\ ^\circ\mathrm{C}, 0.2\% \leqslant \phi_p \leqslant 2\%$	– Curve fitting of the experimental data [69] – TiO_2–water – d_p = 21 nm
Present work	$\mu_{eff} = 0.6002 - 0.569\phi_p + 0.0823\phi_p^2 + 28.8763\frac{\phi_p}{T} - 204.2202\frac{\phi_p^2}{T^2} +$ $561.3175\frac{\phi_p^3}{T^3} 20 \leqslant T(^\circ C) \leqslant 70;\ \phi_p = 0.99\%,\ 2.04\%,\ 3.16\%$	– Curve fitting of Pak and Cho [16] data – TiO_2–Water – d_p = 27 nm – Units: mPa s
Present work	$\mu_{eff} = -0.4262 + \frac{8.4312}{T} + 0.898\phi_p + \frac{524.7147}{T^2} - 0.2217\phi_p^2 - 4.7329\frac{\phi_p}{T} +$ $70.3105\frac{\phi_p^2}{T^2} + 0.0176\phi_p^3 - 5559.4641\frac{\phi_p}{T^3};\ 1\% \leqslant \phi_p \leqslant 9\%,\ 20 \leqslant T(^\circ\mathrm{C}) \leqslant 70$	– Curve fitting of Nguyen et al. [60] data – CuO–water d_p = 29 nm – Units: mPs s
Namburu et al. [71]	$Log(\mu_{eff}) = Ae^{-BT}$, in mm Pa s $A = 1.8375\phi_p^2 - 29.643\phi_p + 165.56$ $B = 4\times10^{-6}\phi_p^2 - 0.001\phi_p + 0.0186$	CuO–ethylene glycol and water mixture1 $\leqslant \phi_p \leqslant 6\%,\ d_p = 29$ nm,$238 < T < 323$ K
Kulkarni et al. [62,63]	$\ln\mu_{eff} = A(\frac{1}{T}) - B$, in mm Pa s $A = 20587\phi_p^2 + 15857\phi_p + 1078.3$ $B = -107.12\phi_p^2 + 53.54\phi_p + 2.8715$	– CuO–water $0.05 \leqslant \phi_p \leqslant 0.15$ d_p = 29 nm $278 \leqslant T \leqslant 323$ K Shear rate = 100 1/s
Koo and Kleinstreuer [72]	$\mu_{eff} = \mu_{static} + \mu_{Brownian}$ $\mu_{Brownian} = 5\times10^4\beta\rho_f\phi_p\sqrt{\frac{KT}{\rho_p d_p}}f(\phi_p, T)$ $f(\phi_p, T) = (-6.04\phi + 0.4705)T + (1722.3\phi_p - 134.63)$ $\beta = \begin{cases} 0.0137(100\phi_p)^{-0.8229} & \phi_p < 0.01 \\ 0.0011(100\phi_p)^{-0.7272} & \phi_p > 0.01 \end{cases}$ $1\% < \phi_p < 4\%, 300 < T < 325K$	– CuO–water

there are no theoretical results available in the literature that predicts accurately the thermal conductivity of nanofluids. The existing results were generally based on the definition of the effective thermal conductivity of a two-component mixture as follows [73]:

$$k_{eff} = \frac{k_f(1-\phi_p)(dT/dx)_f + k_p\phi_p(dT/dx)_p}{\phi_p(dT/dx)_p + (1-\phi_p)(dT/dx)_f}, \tag{16}$$

where $(dT/dx)_f$ is the temperature gradient within the fluid and $(dT/dx)_p$ is the temperature gradient through the particle. The Maxwell model [74] was one the first models proposed for solid–liquid mixture with relatively large particles. It was based on the solution of heat conduction equation through a stationary random suspension of spheres. The effective thermal conductivity is given by:

$$k_{eff} = \frac{k_p + 2k_f + 2\phi_p(k_p - k_f)}{k_p + 2k_f - \phi_p(k_p - k_f)}k_f = k_f + \frac{3\varphi_p(k_p - k_f)}{k_p + 2k_f - \phi_p(k_p - k_f)}, \tag{17}$$

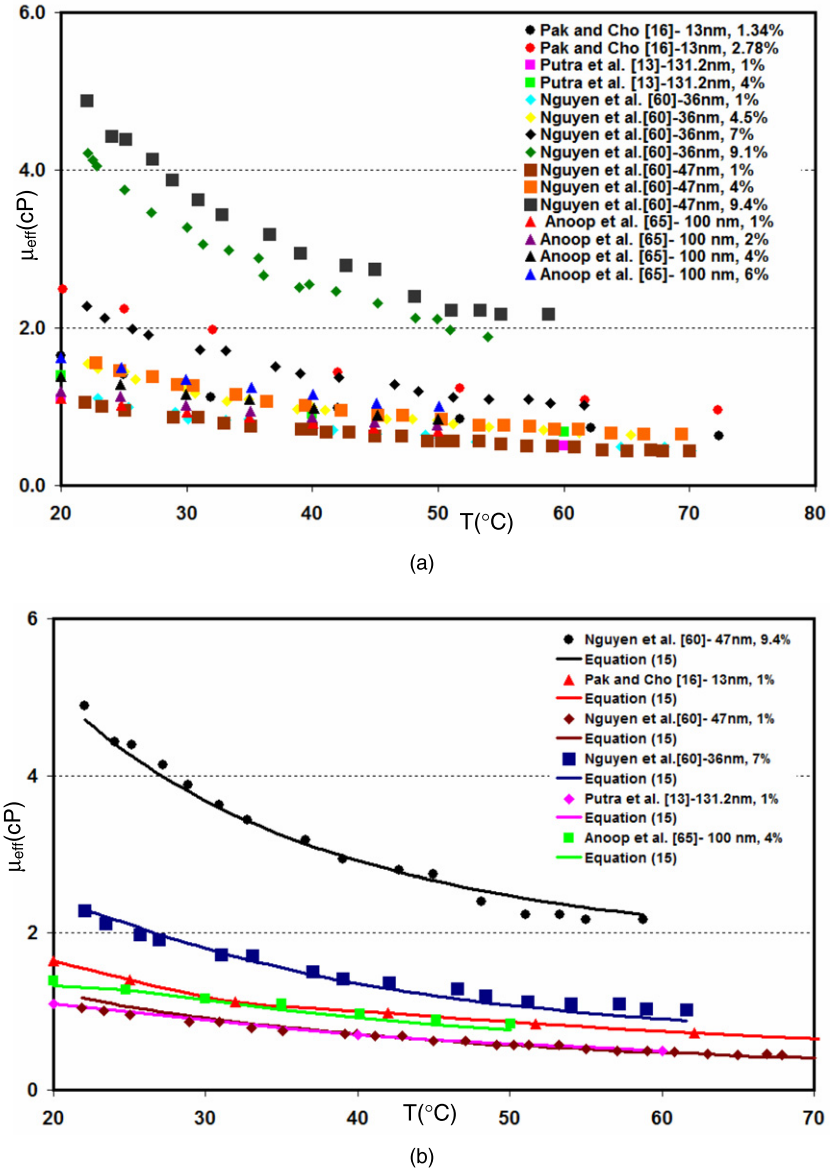

Fig. 5. Effect of the volume fraction and temperature on the effective viscosity of Al_2O_3–water nanofluid (a) experimental measurements; (b) comparison of Eq. (15) developed in the current work with the experimental data.

where k_p is the thermal conductivity of the particles, k_f is the fluid thermal conductivity, and ϕ_p is the volume fraction of the suspended particles. Maxwell model is accurate to order ϕ_p^1 and applicable to $\varphi_p \ll 1$ or $\left|\frac{k_p}{k_f} - 1\right| \ll 1$. Bruggeman [75] proposed a model to study the interactions between randomly distributed spherical particles. The Bruggeman model can be expressed as:

$$\frac{k_{eff}}{k_f} = \frac{(3\phi_p - 1)\frac{k_p}{k_f} + \{3(1-\phi_p) - 1\} + \sqrt{\Delta}}{4}; \quad \Delta = \left[(3\phi_p - 1)\frac{k_p}{k_f} + \{3(1-\phi_p) - 1\}\right]^2 + 8\frac{k_p}{k_f}. \tag{18}$$

The Bruggeman model [75] is applicable for large volume fraction of spherical particles. For low volume fractions, the Bruggeman model [75] results in approximately the same results as the Maxwell model [74]. For non-spherical particles, Hamilton and Crosser [73] developed a model for the effective thermal conductivity of two-component mixtures. Their model was a function of the thermal conductivity of both the base fluid and the particle, volume fraction of the particles, and the shape of the particles. For the thermal conductivity ratio of two phases larger than 100 ($k_p/k_f > 100$), the thermal conductivity of two-component mixtures can be expressed as follows [73]:

$$k_{eff} = \frac{k_p + (n-1)k_f + (n-1)\phi_p(k_p - k_f)}{k_p + (n-1)k_f - \phi_p(k_p - k_f)}k_f, \tag{19}$$

where n is the empirical shape factor given by $n = 3/\psi$, and ψ is the particle sphericity, defined by the ratio of the surface area of a sphere with volume equal to that of the particle, to the surface area of the particle. Maxwell's model [74] is a special case of Hamilton and Crosser's model for sphericity equal to one (for spheres: $n = 3$). The shape factor for cylinders is $n = 6$. Apparently, the most notable drawback of the Hamilton Crosser model [73] is that important physical parameters such as temperature and particle size are not considered. Tables 5–7 summarize some pertinent models for the effective thermal conductivity of nanofluids including the effects of Brownian motion and nano-layer.

Table 5
Summary of theoretical models for the effective thermal conductivity of nanofluids.

Models	Expressions	Physical model	Remarks
Maxwell [74]	$\frac{k_{eff}}{k_f}=\frac{k_p+2k_f+2\phi_p(k_p-k_f)}{k_p+2k_f-\phi_p(k_p-k_f)}$	– Based on the conduction solution through a stationary random suspension of spheres	– Spherical particles – Accurate to order ϕ_p^1
Bruggeman [75]	$\frac{k_{eff}}{k_f}=\frac{(3\phi_p-1)\frac{k_p}{k_f}+\{3(1-\phi_p)-1\}+\sqrt{\Delta}}{4}$ $\Delta=[(3\phi_p-1)\frac{k_p}{k_f}+\{3(1-\phi_p)-1\}]^2+8\frac{k_p}{k_f}$	– Based on the differential effective medium (DEM) theory to estimate the effective thermal conductivity of composites at high particle concentrations – It consists in building up the composite medium through a process of incremental homogenization	– Applicable to high volume fraction of spherical particles – Suspension with spherical inclusions – No shape factor
Hamilton–Crosser [73]	$\frac{k_{eff}}{k_f}=\frac{k_p+(n-1)k_f+(n-1)\phi_p(k_p-k_f)}{k_p+(n-1)k_f-\phi_p(k_p-k_f)}$	– Based on the effective thermal conductivity of a two-component mixture	– Spherical and non-spherical particles – $n=3$ (spheres), $n=6$ (cylinders)
Wasp [76]	$\frac{k_{eff}}{k_f}=\frac{k_p+2k_f+2\phi_p(k_p-k_f)}{k_p+2k_f-\phi_p(k_p-k_f)}$	– Based on effective thermal conductivity of a two-component mixture	– Special case of Hamilton and Crosser's model with $n=3$
Jeffery [77]	$\frac{k_{eff}}{k_f}=1+3\eta\phi_p+\phi_p^2\left(3\eta^2+\frac{3\eta^2}{4}+\frac{9\eta^3}{16}\frac{\kappa+2}{2\kappa+3}+\ldots\right)$ $\kappa=\frac{k_p}{k_f},\eta=\frac{\kappa-1}{\kappa+2}$	– Based on the conduction solution through a stationary random suspension of spheres	– High order terms represent pair interactions of randomly dispersed spherical particles – Accurate to order ϕ_p^2
Davis [78]	$\frac{k_{eff}}{k_f}=1+\frac{3(\kappa-1)}{(\kappa+2)-\phi_p(\kappa-1)}[\phi_p+f(\kappa)\phi_p^2+O(\phi_p^3)]$	– Green's theorem was applied to the space occupied by the matrix material (spherical inclusions) – Decaying temperature field was used	– Accurate to order ϕ_p^2 – High order terms represent pair interactions of randomly dispersed particles – $f(\kappa)=2.5$ for $\kappa=10$; $f(\kappa)=0.5$ for $\kappa=\infty$
Lu and Lin [79]	$\frac{k_{eff}}{k_f}=1+a\phi_p+b\phi_p^2$	– The effective conductivity of composites containing aligned spheroids of finite conductivity was modeled with the pair interaction – The pair interaction was evaluated by solving a boundary value problem involving two aligned spheroids	– Spherical and non-spherical particles – Spherical particles: $a=2.25$, $b=2.27$ for $\kappa=10$; $a=3$, $b=4.51$ for $\kappa=\infty$

Table 6
Summary of theoretical models for the effective thermal conductivity of nanofluids (nano-layer effect).

Models	Expressions	Physical model	Remarks
Yu and Choi [33]	$k_{eff}=\frac{k_{pe}+2k_f+2\phi_p(k_{pe}-k_f)(1+\beta)^3}{k_{pe}+2k_f-\phi_p(k_{pe}-k_f)(1+\beta)^3}k_f$ $k_{pe}=\frac{2(1-\gamma)+(1+\beta)^3(1+2\gamma)\gamma}{-(1-\gamma)+(1+\beta)^3(1+2\gamma)}k_p$ ($\beta=t/r_p$) and $\gamma(=k_{layer}/k_p)$	– Modified Maxwell model [74]	– Spherical particles – Nano-layer
Yu and Choi [34]	$k_{eff}=\left(1+\frac{nf_eA}{1-f_eA}\right)k_f$ $A=\frac{1}{3}\sum_{j=a,b,c}\frac{(k_{pj}-k_f)}{k_{pj}+(n-1)k_f}$ $f_e=\frac{f\sqrt{(a^2+t)(b^2+t)(c^2+t)}}{abc}$	– Modified Hamilton–Crosser model [73]	– Non spherical particles – Nano-layer
Xue [36]	$9\left(1-\frac{\phi_p}{\lambda}\right)\frac{k_{eff}-k_f}{2k_{eff}+k_f}+\frac{\phi_p}{\lambda}\frac{k_{eff}-k_{c,x}}{k_{eff}+B_{2,x}(k_{c,x}-k_{eff})}+\frac{\phi_p}{\lambda}4\frac{k_{eff}-k_{c,y}}{2k_{eff}+(1-B_{2,x})(k_{c,y}-k_{eff})}=0$	– Based on the Maxwell model and the average polarization theory and on the assumption that there is an interfacial shell between the nanoparticles and the base fluid	– Spherical particles – Nano-layer
Xue and Xu [35]	$\left(1-\frac{\phi_p}{\alpha}\right)\frac{k_{eff}-k_f}{2k_{eff}+k_f}+\frac{\phi_p}{\alpha}\frac{(k_{eff}-k_{shell})(2k_{shell}+k_p)-\alpha(k_p-k_{shell})(2k_{shell}+k_{eff})}{(2k_{eff}+k_{shell})(2k_{shell}+k_p)+2\alpha(k_p-k_{shell})(k_{shell}-k_{eff})}=0$	– A modified Bruggeman model [75] including the effect of interfacial shells	– Spherical particles – Nano-layer
Xie et al. [37]	$\frac{k_{eff}-k_f}{k_f}=3\Theta\phi_T+\frac{3\Theta^2\phi_T^2}{1-\Theta\phi_T}$ $\phi_T=\frac{4}{3}\pi(r_p+t)^3N_p=\phi_p(1+\beta)^3,\beta=\frac{t}{r_p}$	– Based on Fourier's law of heat conduction	– Low particle loadings – Nano-layer

5.1. Experimental investigations

Several experimental studies were conducted in the literature to measure the thermal conductivity of nanofluids using different techniques such as transient hot wire, steady-state parallel plates, and temperature oscillation. Despite numerous studies motivated by the significant benefits of utilizing nanofluids in various applications, the pertinent mechanisms of the thermal conductivity enhancement of nanofluids have not been well understood. Moreover, published results demonstrate thermal conductivity enhancement varying from anomalously large to small values as shown in Table 8. Table 8 shows a comparison of the experimental thermal conductivity enhancements of Al_2O_3 nanofluids cited in the literature. Al_2O_3 and CuO are the most common nanoparticles used in the literature.

Several studies have reported enhancement in the thermal conductivity of nanofluids at room temperature [84]. Fig. 6a and b show the effective thermal conductivity measurements at ambient temperature for Al_2O_3–water and CuO–water nanofluids at various volume concentrations and nanoparticle diameters. Fig. 9 shows that the effective thermal conductivity increases with an increase in the volume fraction. In addition, the size of the particles is found to have a significant effect on the thermal conductivity enhancement. It should be noted that smaller particles exhibit larger surface area – to – volume ratio than the larger particles. As such, smaller particle diameters can possibly result in a larger augmentation in the effective thermal conductivity. It is interesting to note from Fig. 6a and b that the Hamilton–Crosser model [73] may represent a good approximation for the effective thermal conductivity value for smaller volume fractions ($\phi_p \leqslant 4\%$).

Table 7
Summary of theoretical models for the effective thermal conductivity of nanofluids (Brownian effect).

Models	Expressions	Physical model	Remarks
Wang et al. [19]	$\frac{k_{eff}}{k_f}=\frac{(1-\phi_p)+3\phi_p\int_0^\infty \frac{k_{cl}(r)n(r)}{k_{cl}(r)+2k_f}dr}{(1-\phi_p)+3\phi_p\int_0^\infty \frac{k_f(r)n(r)}{k_{cl}(r)+2k_f}dr}$	– Based on the effective medium approximation and the fractal theory for predicting the thermal conductivity of nanofluids	– Accounts for the size effect and the surface adsorption of nanoparticles
Xuan et al. [80]	$\frac{k_{eff}}{k_f}=\frac{k_p+2k_f-2\phi_p(k_f-k_p)}{k_p+2k_f+\phi_p(k_f-k_p)}+\frac{\rho_p\phi_p c_p}{2k_f}\sqrt{\frac{k_BT}{3\pi r_c\mu}}$	– Based on Maxwell model – The theory of Brownian motion and the diffusion-limited aggregation model are applied to simulate random motion and the aggregation process of the nanoparticles	– Includes the effect of random motion, particle size, concentration, and temperature
Jang and Choi [10]	$k_{eff}=k_f(1-\phi_p)+k_p\phi_p+3C\frac{d_f}{d_p}k_f\mathrm{Re}_{d_p}^2\mathrm{Pr}\phi_p$	– A theoretical model was developed based on kinetics, Kapitza resistance, and convection – A general expression for the thermal conductivity of nanofluids involving four modes of energy transport in nanofluids was derived	– Considered four modes of energy transport: collision between fluid molecules, thermal diffusion of nanoparticles, collision between nanoparticles due to Brownian motion, and thermal interactions of dynamic nanoparticles with fluid molecules – Collision of nanoparticles due to Brownian motion is neglected
Prasher et al. [81]	$k_{eff}=(1+A\mathrm{Re}^m\mathrm{Pr}^{0.333}\phi_p)\times[\frac{k_p+2k_f+2\phi_p(k_p-k_f)}{k_p+2k_f-\phi_p(k_p-k_f)}]k_f$	– Based on Maxwell model and heat transfer in fluidized beds	– Accounts for convection caused by the Brownian motion from multiple nanoparticles
Koo and Kleinstreuer [72,82]	$k_{eff}=k_{static}+k_{Brownian}=\frac{k_p+2k_f+2\phi_p(k_p-k_f)}{k_p+2k_f-\phi_p(k_p-k_f)}k_f+5\times10^4\beta\phi_p\rho_p c_p\sqrt{\frac{k_BT}{\rho_p D}}f(T,\phi_p)$	– Based on Maxwell model – Curve fitting of the available experimental data to determine the effective conductivity due to Brownian motion	– Considered surrounding liquid traveling with randomly moving nanoparticles
Chon et al. [83]	$\frac{k_{eff}}{k_f}=1+64.7\phi_p^{0.74}(\frac{d_f}{d_p})^{0.369}(\frac{k_p}{k_f})^{0.747}\times\mathrm{Pr}^{0.9955}\mathrm{Re}^{1.2321}$ $\mathrm{Pr}=\frac{\mu_f}{\rho_f\alpha_f}$, $\mathrm{Re}=\frac{\rho_f V_{Br}d_p}{\mu_f}=\frac{\rho_f k_B T}{3\pi\mu_f^2 l_f}$	– Based on the curve fitting of the experimental data	– Reynolds number is based on the Brownian motion velocity

Table 8
Comparison of the experimental thermal conductivity enhancements of Al_2O_3 nanofluids cited in the literature.

	Base fluid	D_p	ϕ_p (%)	%Thermal conductivity enhancement	Method
[22]	Water	38.4 nm	4	9.4% (21 °C), 24.3% (51 °C)	Temperature Oscillation
[13]	Water	131 nm	4	24% (51 °C)	Steady-state parallel plates
[56]	Water	13 nm	4.4	33%	Transient hot wire
[85]	Water	38.4 nm	4.3	11%	Transient hot wire
[85]	EG*	38.4	5	19%	Transient hot wire
[55]	Water	28 nm	5.5	16%	Steady-state parallel plates
[55]	EG	28 nm	5	24.5%	Steady-state parallel plates
[83]	Water	11 nm	1	14.8% (70 °C)	Transient hot wire
[83]	Water	47 nm	1	10.2% (70 °C)	Transient hot wire
[83]	Water	150 nm	1	4.8% (60 °C)	Transient hot wire
[83]	Water	47 nm	4	28.8 % (70 °C)	Transient hot wire
[86]	Water	36 nm	6	28.2%	Steady-state parallel plates
[86]	Water	47 nm	6	26.1%	Steady-state parallel plates
[87]	Water	20 nm	5	15%	Transient hot wire
[88]	Water	11 nm	5	8%	Transient hot wire
[88]	Water	20 nm	5	7%	Transient hot wire
[88]	Water	40 nm	5	10%	Transient hot wire

* EG: ethylene glycol.

A general correlation for the effective thermal conductivity of Al_2O_3–water and CuO–water nanofluids at ambient temperature accounting for various volume fractions and nanoparticles diameters is obtained by the present authors using the available experimental data in the literature. This model can be expressed as:

$$\frac{k_{eff}}{k_f}=1.0+1.0112\phi_p+2.4375\phi_p\left(\frac{47}{d_p(\mathrm{nm})}\right)-0.0248\phi_p\left(\frac{k_p}{0.613}\right);\quad R^2=96.5\%, \tag{20}$$

where k_f is the thermal conductivity of water. Fig. 7 demonstrates that the general correlation, represented by Eq. (20), is in good agreement with the experimental measurements of Al_2O_3–water and CuO–water nanofluids.

Thermal conductivity measurements at different temperatures are essential because the measurements at ambient temperature are not adequate for estimating the heat transfer characteristics. Fig. 8 shows a comparison of the relative effective thermal conductivity (ratio of the effective thermal conductivity of the nanofluid to the thermal conductivity of the base fluid at the same temperature) results of Al_2O_3–water nanofluid obtained from various experimental results as a function of volume fraction and nanoparticle's diameter. Fig. 8 shows that temperature has a significant

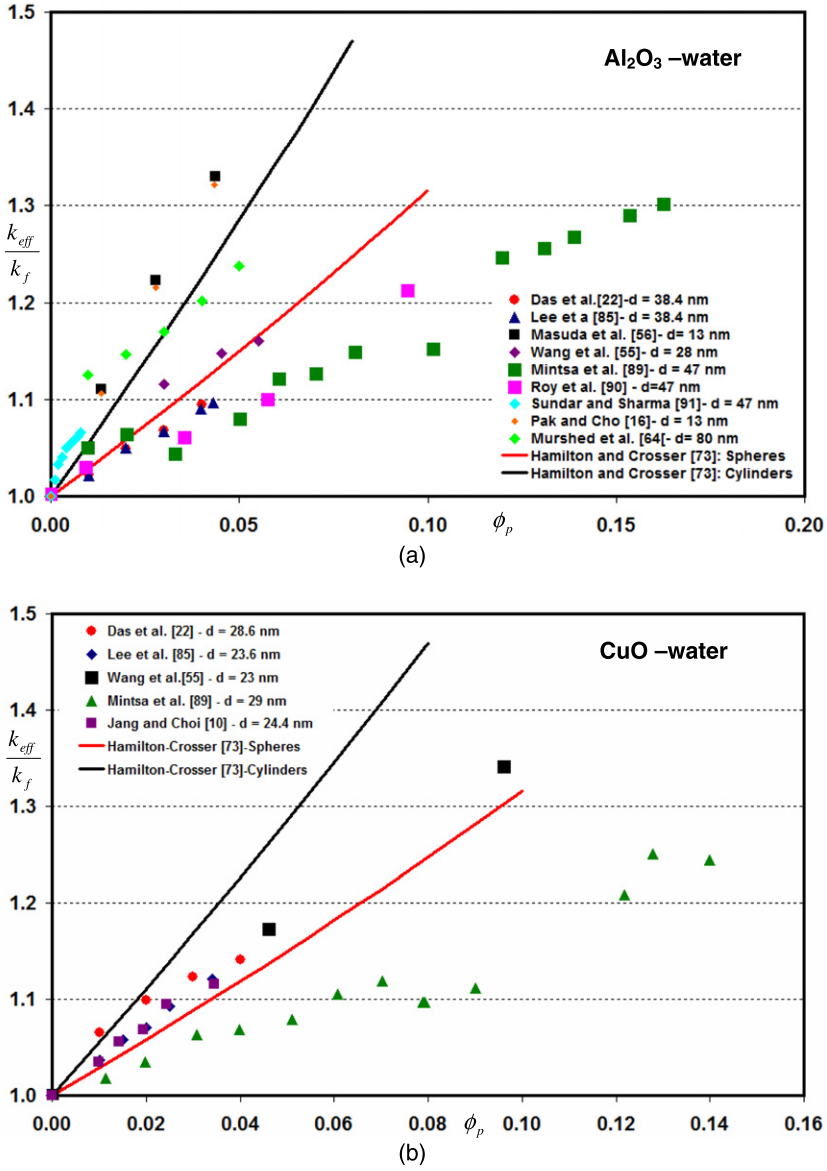

Fig. 6. Effect of the volume fraction on the effective thermal conductivity measurements (a) Al_2O_3–water; (b) CuO–water. (See above-mentioned references for further information.)

effect on the thermal conductivity enhancement. A general correlation is developed for Al_2O_3–water nanofluid by the present authors using the available experimental data at various temperatures, nanoparticle's diameter, and volume fraction. The developed correlation is expressed in terms of nanoparticle's diameter, volume fraction, dynamic viscosity of water, effective dynamic viscosity of the nanofluid, and temperature as follows:

$$\frac{k_{eff}}{k_f} = 0.9843 + 0.398\phi_p^{0.7383}\left(\frac{1}{d_p(\mathrm{nm})}\right)^{0.2246}\left(\frac{\mu_{eff}(T)}{\mu_f(T)}\right)^{0.0235} - 3.9517\frac{\phi_p}{T} + 34.034\frac{\phi_p^2}{T^3} + 32.509\frac{\phi_p}{T^2}\quad 0 \leqslant \phi_p \leqslant 10\%,\quad 11\ \mathrm{nm} \leqslant d \leqslant 150\ \mathrm{nm},\ 20\ ^\circ\mathrm{C} \leqslant T \leqslant 70\ ^\circ\mathrm{C}, \tag{21}$$

where the dynamic viscosity (Pa s) of water at different temperatures can be expressed as:

$$\mu_f(T) = 2.414 \times 10^{-5} \times 10^{247.8/(T-140)}.$$

The validity of the above correlation (Eq. (21)) is depicted in Fig. 9. Fig. 9 shows a very good agreement between the predicted relative effective thermal conductivity by our model and the experimental data.

Different models were developed in the past for the effective thermal conductivity of a two-component mixture such as Hamilton–Crosser model [73]. Although this model gave a good approximation for the effective thermal conductivity of the Al_2O_3–water and CuO–water nanofluids for small volume fractions at room temperature, it does not provide a good approximation of the effective thermal conductivity at various temperatures shown in Fig. 9 because this model as well as a number of other models in this area do not properly account for the variations of the effective thermal conductivity with temperature. Therefore, these analytical models cannot be used to determine the effective thermal conductivity of nanofluids at various temperatures. Instead, Eq.

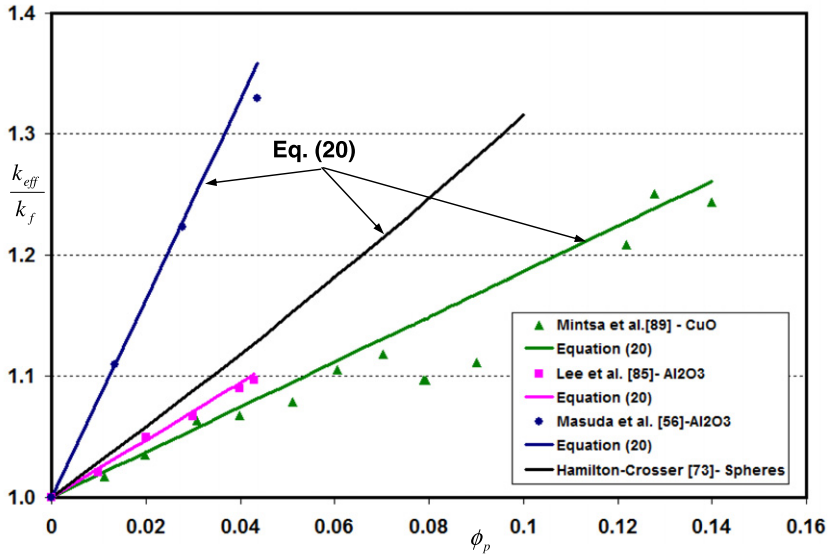

Fig. 7. Comparison of the general correlation, Eq. (20) developed in the current work, with the experimental data (Al_2O_3–water, CuO–water) at room temperature.

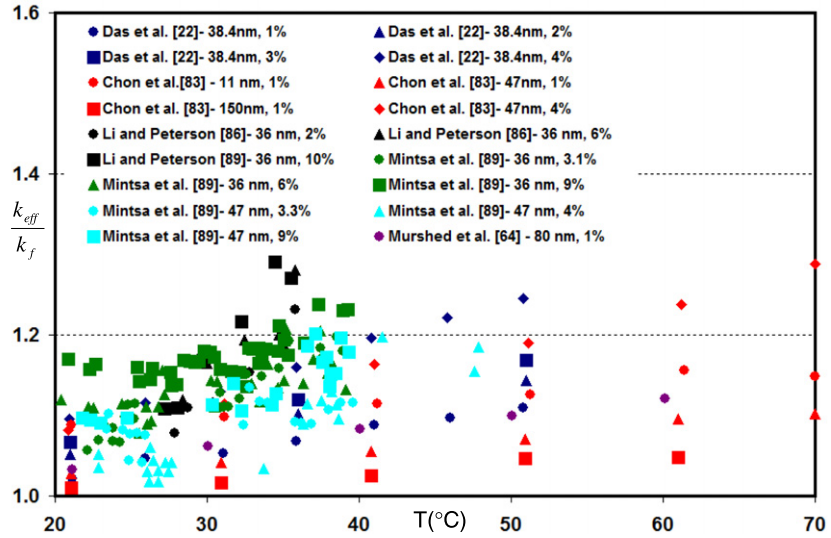

Fig. 8. Comparison of the experimental data for the thermal conductivity enhancement of Al_2O_3–water nanofluid at different temperatures and volume fractions.

(21) developed in this work should be used. Table 9 summarizes all the correlations that were developed in the present work for nanofluids.

5.2. Natural convection heat transfer utilizing nanofluids

Conflicting results were reported in the literature regarding natural convection heat transfer enhancement using nanofluids. The findings of both experimental and analytical investigations are still in disagreement. Analytical studies show an increase in heat transfer with an increase in the volume fraction of nanoparticles which is not in agreement with the experimental results. Since Rayleigh number, which is the ratio of the buoyancy to the viscous forces, represents a significant parameter in natural convection processes, comparison of nanofluid Rayleigh number to the base fluid Rayleigh number at various volume fractions and temperature is highlighted in this section. Using a scale analysis approach, the viscous and buoyancy forces can be expressed as:

$$\text{Viscous force}: \quad \frac{\nu}{H^3}\alpha \ (\text{N/kg}), \tag{22}$$

$$\text{Buoyancy force}: \quad g\beta\Delta T \ (\text{N/kg}). \tag{23}$$

The ratio of nanofluid Rayleigh number to that of the base fluid can then be expressed as:

$$\frac{Ra_{nf}}{Ra_f} = \frac{\beta_{nf}}{\beta_f}\frac{\nu_f}{\nu_{nf}}\frac{\alpha_f}{\alpha_{nf}}. \tag{24}$$

Fig. 10a shows that the ratio of the Rayleigh number of nanofluid to that of the base fluid decreases with an increase in the Al_2O_3 volume fraction. Higher volume fractions of the solid nanoparticles causes an increase in the viscous force of nanofluids and consequently suppresses heat transfer. Moreover, Fig. 10a shows the effect of varying particle diameter on the Rayleigh number ratio. As the particle diameter increases, the ratio of the Rayleigh numbers decreases because the effective thermal conductivity of nanofluids decreases and the kinematic viscosity increases with an increase in the size of nanoparticles. However, the rate of

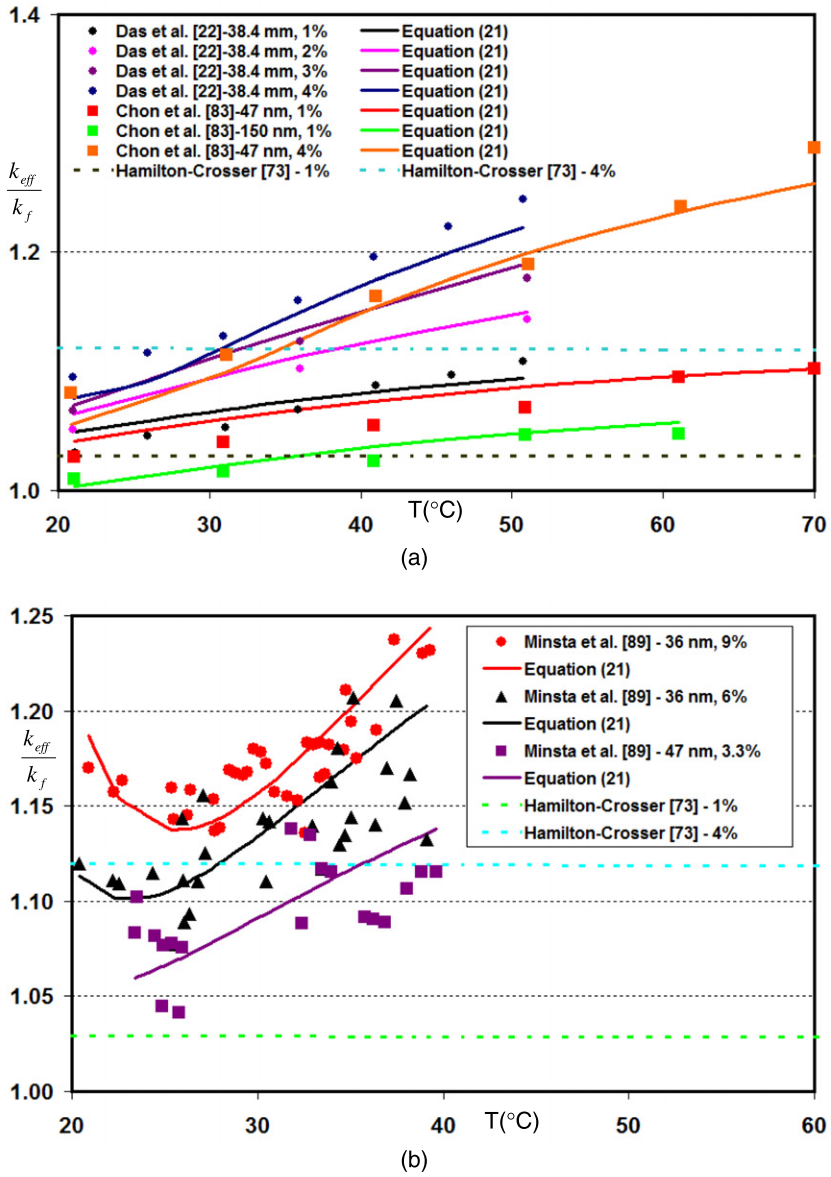

Fig. 9. Comparison of the general correlation, Eq. (21) developed in the current work, with the experimental data (Al_2O_3–water) at various temperatures and volume fractions (a) Das et al. [22] and Chon et al. [83]; (b) Minsta et al. [89].

increase of the kinematic viscosity of the nanofluid with the particle size is larger than the resulting decrease of the effective thermal conductivity. This may provide a physical reason for the reduction of natural convection heat transfer enhancement with an increase in the volume fraction of nanoparticles at room temperature.

The effect of varying the temperature of nanofluids and volume fraction on the ratio of Rayleigh numbers is illustrated in Fig. 10b for nanoparticles diameter of 36 nm. Fig. 10b shows that the ratio of nanofluid Rayleigh number to the base fluid Rayleigh number increases with an increase in the temperature. Moreover, this ratio is higher for volume fraction of 1% compared to 4% for various temperatures. This is because the kinematic viscosity and the effective thermal conductivity of nanofluids increase with an increase in the volume fraction of nanoparticles. For volume fraction of 1%, Fig. 10b shows an interesting result associated with the fact that nanofluid Rayleigh number is smaller than the Rayleigh number of water base below 31 °C. For temperatures greater than 31 °C, Fig. 10b shows that nanofluid Rayleigh number is higher than that of the base water. Hence, nanofluids may exhibit natural convection heat transfer enhancement at high temperatures. This is associated with the behavior of the kinematic viscosity and the thermal diffusivity for both nanofluid and the base water at various temperatures as shown in Fig. 11. Hence, Fig. 10a and b shows that natural convection heat transfer is not exclusively characterized by the effective thermal conductivity of nanofluids but also depends on the viscosity of nanofluids.

5.3. Surface tension

Studies on surface tension of nanofluids are limited in the literature [92–96]. Golubovic et al. [92] showed experimentally that the surface tension of Al_2O_3–water nanofluid does not change for concentrations of nanoparticles considered in their work (0–0.01 g/l) and the surface tension is approximately equal to surface tension of pure water at $T = 24$ °C. Xue et al. [93] showed insignificant effect of carbon nanotube nanofluid on surface tension

Table 9
Summary of the correlations developed in the present work.

Physical properties	Room temperature	Temperature dependent
Density	$\rho_{eff} = (1-\varphi_p)\rho_f + \varphi_p\rho_p$	$\rho_{eff} = 1001.064 + 2738.6191\phi_p - 0.2095T0 \leqslant \phi_p \leqslant 0.04, 5 \leqslant T(^\circ C) \leqslant 40$
Specific hat	$c_{eff} = \frac{(1-\phi_p)\rho_f c_f + \phi_p\rho_p c_p}{\rho_{eff}}$	N/A
Thermal expansion coefficient	$\beta_{eff} = \frac{(1-\phi_p)(\rho\beta)_f + \phi_p(\rho\beta)_p}{\rho_{eff}}$	$\beta_{eff} = (-0.479\phi_p + 9.3158\times10^{-3}T - \frac{4.7211}{T^2})\times10^{-3}$
	$\beta_{eff} = (1-\phi_p)\beta_f + \phi_p\beta_p$	$0 \leqslant \phi_p \leqslant 0.04, 10^\circ C \leqslant T \leqslant 40^\circ C$
Viscosity	N/A	– Al_2O_3
		$\mu_{eff} = -0.4491 + \frac{28.837}{T} + 0.574\phi_p - 0.1634\phi_p^2 + 23.053\frac{\phi_p^2}{T^2} + 0.0132\phi_p^3$
		$-2354.735\frac{\phi_p}{T^3} + 23..498\frac{\phi_p^2}{d_p^2} - 3.0185\frac{\phi_p^3}{d_p^2}$
		$1\% \leqslant \phi_p \leqslant 9\%, 20 \leqslant T(^\circ C) \leqslant 70, 13\text{ nm} \leqslant d_p \leqslant 131\text{ nm}$
Thermal conductivity	– Al_2O_3 and CuO	– Al_2O_3
	$\frac{k_{eff}}{k_f} = 1.0 + 1.0112\phi_p + 2.4375\phi_p\left(\frac{47}{d_p(nm)}\right) - 0.0248\phi_p\left(\frac{k_p}{0.613}\right)$	$\frac{k_{eff}}{k_f} = 0.9843 + 0.398\phi_p^{0.7383}\left(\frac{1}{d_p(nm)}\right)^{0.2246}\left(\frac{\mu_{eff}(T)}{\mu_f(T)}\right)^{0.0235} - 3.9517\frac{\phi_p}{T} + 34.034\frac{\phi_p^2}{T^3} + 32.509\frac{\phi_p}{T^2}$
		$0 \leqslant \phi_p \leqslant 10\%, 11\text{ nm} \leqslant d \leqslant 150\text{ nm}, 20^\circ C \leqslant T \leqslant 70^\circ C$

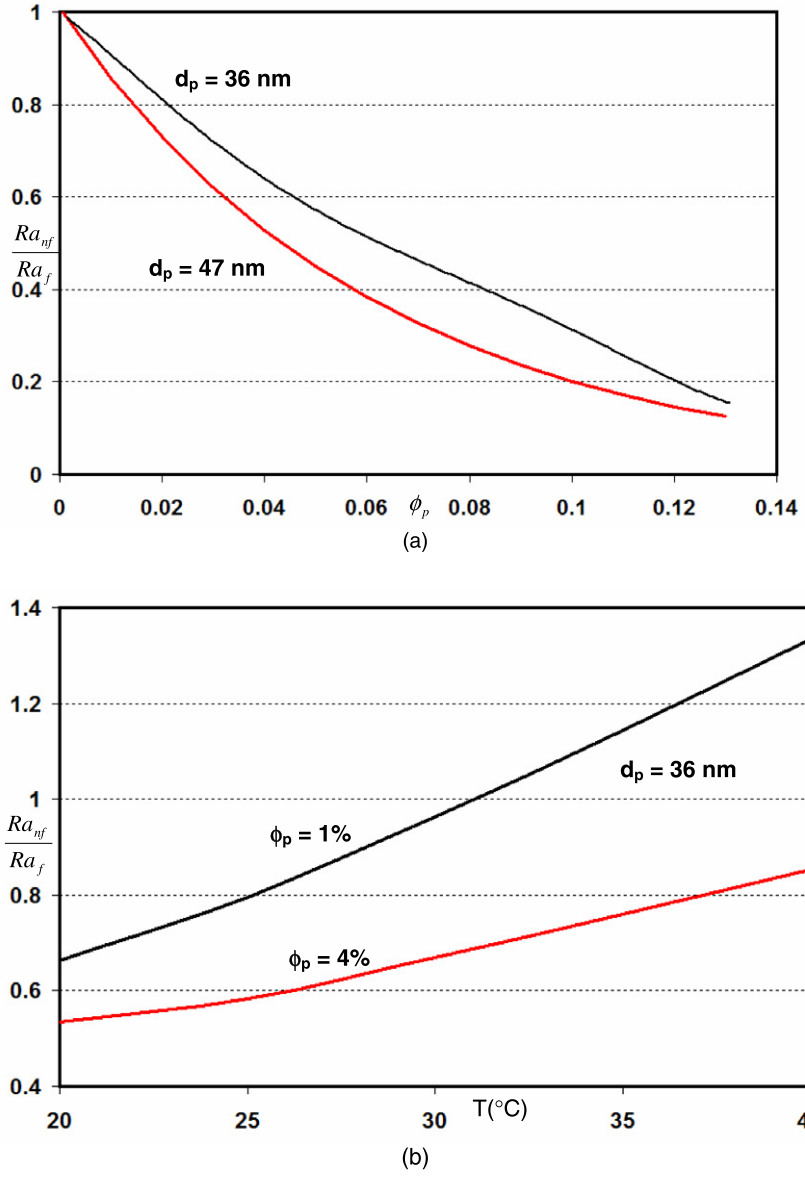

Fig. 10. Effect of volume fraction and temperature on the ratio of the Rayleigh numbers for different particle diameters (Al_2O_3–water nanofluid) (a) room temperature; (b) various temperatures.

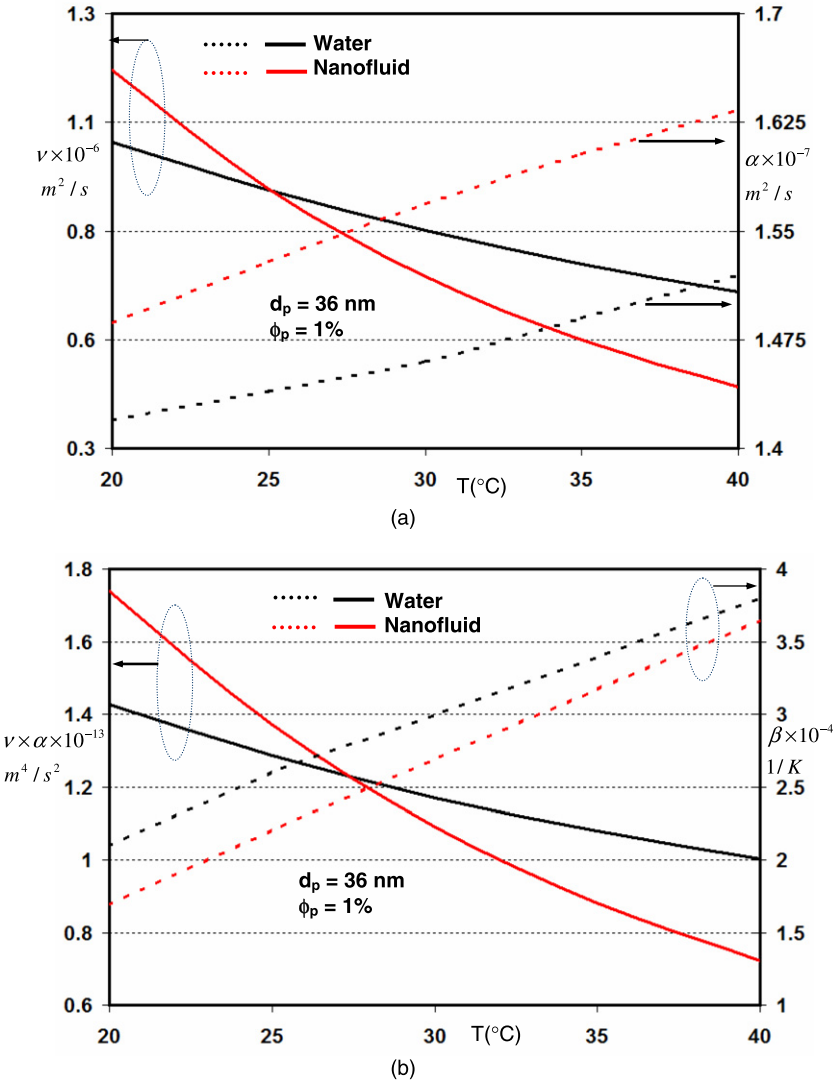

Fig. 11. Effect of varying temperature on the thermophysical properties (a) Al_2O_3–water nanofluid; (b) water.

compared with pure water. Similarly, Kim et al. [94] found that the surface tension of Al_2O_3–water nanofluids (0.1% volume fraction) differed negligibly from those of pure water. The effect of temperature on the surface tension of nanofluids was studied by Murshed et al. [95]. Their experimental results showed that nanofluids having TiO_2 nanoparticles of 15 nm diameter in deionized water exhibit substantially lower surface tension than those of the base fluid (i.e. deionized water). Similarly, Zhu et al. [96] showed that the surface tension of nanofluids was highly dependent on the temperature. One can note from the above that as expected temperature plays a significant role on the surface tension of nanofluids.

5.4. Nucleate pool boiling and critical heat flux (CHF) of Nanofluids

Several experimental studies on the nucleate pool boiling and CHF characteristics of nanofluids have been investigated in the literature. Many researchers expected that the addition of nanoparticles would have a potential to enhance the boiling heat transfer characteristics. Conflicting results were reported on the effect of the nanoparticles concentration on the pool boiling characteristics of nanofluids. Some studies have shown that the addition of nanoparticles exhibited a decrease or no change in the nucleate boiling heat transfer rate [20,21,97–99] while other studies have illustrated an increase [100–103]. However, most CHF experiments using nanofluids were in agreement in reporting an enhancement in CHF for pool boiling conditions [98,99,104,105]. The mechanism for the CHF enhancement may be attributed to the deposition and sintering of nanoparticles on the boiling surfaces resulting in an increase in the nucleation sites [98]. For example, Kim et al. [94] conducted an experimental study on the CHF characteristics of nanofluids in pool boiling. Their results show that the CHF of nanofluids containing TiO_2 or Al_2O_3 were enhanced up to 100% over that of pure water.

You et al. [98] conducted an experimental study to determine the boiling curve and the CHF at pool boiling conditions from a flat square polished copper heater immersed in Al_2O_3–water nanofluid at various volume fractions ranging between 0.0 g/l and 0.05 g/l. Their results illustrate a drastic enhancement in the CHF for Al_2O_3–water nanofluids (~200% higher than pure water; measured in nanofluids containing 0.005 g/l of Al_2O_3 nanoparticles). However, heat transfer enhancement or degradation was not observed in the nucleate boiling regime for nanofluids. For example, Vassallo et al. [106] experimentally demonstrated a marked increase in the CHF for both nano- and micro-solutions (silica–water) at the same concentration (0.5% volume fraction) compared to the base water. However, from boiling curves data, no heat transfer enhancement of nanofluids was observed in the nucleate boiling regime.

5.5. Nucleate pool boiling heat transfer and CHF mechanisms of nanofluids

Several studies have been conducted in the literature to explore the enhancement mechanisms or deterioration of nucleate pool boiling heat transfer using nanofluids. These mechanisms include formation of nanoparticles coatings on the surface during pool boiling of nanofluids [99], decrease in active nucleation sites due to nanoparticle sedimentation on the boiling surface [107], and the wettability change of the surface [20,21]. The available experimental results on nucleate pool boiling heat transfer coefficient of nanofluids are in disagreement. While the CHF enhancement results by nanofluids are consistent in the literature, the responsible mechanisms are not verified. Golubovic et al. [92] concluded that the major reason behind the increase of CHF in pool boiling of nanofluids is a decrease in the static surface contact angle.

Many other studies consider the primary reason for CHF enhancement is due to the surface coating effect [99,100,106,108–111]. For example, Bang and Chang [99] conducted an experimental study on boiling heat transfer characteristics of nanofluids with nanoparticles suspended in water using different concentrations of alumina nanoparticles. The CHF performance was enhanced for both horizontal (32%) and vertical (13%) flat surfaces and the authors related this enhancement to a change of surface characteristics by the deposition of nanoparticles. If this reasoning is accepted, it might be easier to modify the boiling surface in pursuit of a greater number of nucleation sites per area rather than using nanofluids. The CHF enhancement is normally achieved by increasing boiling surface area using a variety of fin shapes and sizes [112,113]. Anderson and Mudawar [112] illustrated that the surfaces with microgrooves and square microstuds are highly effective in enhancing the nucleate boiling heat transfer coefficient in Fluorinert electronic liquid (FC-72) and increasing CHF values by up to 2.5 times compared to a smooth surface. Honda et al. [114] and Wei et al. [115] showed that CHF values for the nano-roughened surface and micro-pin-finned surfaces were respectively 1.8–2.2 and 2.3 times those for a smooth silicon surface. Ujereh et al. [116] performed experiments to assess the impact of coating silicon and copper substrates with nanotubes on pool boiling performance. Fully coating the substrate surface with carbon nanotubes was found to be highly effective at reducing the incipience superheat and significantly enhancing both the nucleate boiling heat transfer coefficient and CHF.

More robust physical models are essential to explain the effect of nanofluids on nucleate pool boiling and CHF. The thermophysical properties of nanofluids such as surface tension, density, viscosity, specific heat, etc; may also have an effect on nucleate pool boiling heat transfer coefficient and CHF. Detailed knowledge of the thermophysical properties of nanofluids, structure of the boiling surface, and coating of nanoparticles can be helpful in resolving the controversies in the pool boiling heat transfer coefficient of nanofluids as well as in illustrating the mechanisms that cause the significant increase in CHF.

6. Conclusions

Thermophysical characteristics of nanofluids and their role in heat transfer enhancement are analyzed in this work. General correlations for the effective thermal conductivity and viscosity of nanofluids are developed based on the pertinent experimental data in terms of the volume fraction, particle diameter, temperature, and the base fluid physical properties. The effective viscosity of nanofluids is found to increase with an increase in the volume fraction and decrease with an increase in the temperature. The effective thermal conductivity of nanofluids increases with an increase in temperature and volume fraction and decreases with an increase in the particle diameter. At room temperature, classical models can be used to estimate the thermal conductivity and viscosity of nanofluids for low volume fractions. However, these models cannot predict the thermal conductivity at other temperatures. Correlations based on available experimental data accounting for the temperature effect are developed in this work. The findings from experimental and analytical investigations are still in disagreement regarding natural convection enhancement utilizing nanofluids. The current work illustrates that the viscosity of nanoflluids plays a key role in predicting the heat transfer characteristics. Differences in thermal conductivity and viscosity measurements in the literature using different measurement techniques are highlighted. Moreover, for high heat flux applications, the experimental results illustrate conflicting results in pool boiling heat transfer characteristics while the critical heat flux of nanofluids shows a significant increase with the addition of nanoparticles. While the addition of nanoparticles appear not to have a significant effect on the surface tension of the nanofluid, experiment show that the surface tension of the nanofluids is significantly dependent on the temperature. Several pertinent correlations for the thermophysical properties of nanofluids were developed in this work based on the available experimental data. This work clearly illustrates the need for additional investigations in measuring the nanofluid properties.

References

[1] S.U.S. Choi, Nanofluids: from vision to reality through research, J. Heat Transfer 131 (2009) 1–9.
[2] K.V. Wong, O. Leon, Applications of nanofluids: current and future, Adv. Mech. Eng. 2010 (2010) 1–11.
[3] V. Bianco, F. Chiacchio, O. Manca, S. Nardini, Numerical investigation of nanofluids forced convection in circular tubes, Appl. Therm. Eng. 29 (2009) 3632–3642.
[4] M. Shafahi, V. Bianco, K. Vafai, O. Manca, Thermal performance of flat-shaped heat pipes using nanofluids, Int. J. Heat Mass Transfer 53 (2010) 1438–1445.
[5] M. Shafahi, V. Bianco, K. Vafai, O. Manca, An investigation of the thermal performance of cylindrical heat pipes using nanofluids, Int. J. Heat Mass Transfer 53 (2010) 376–383.
[6] K. Khanafer, K. Vafai, M. Lightstone, Buoyancy-driven heat transfer enhancement in a two-dimensional enclosure utilizing nanofluids, Int. J. Heat Mass Transfer 46 (2003) 3639–3653.
[7] A.R.A. Khaled, K. Vafai, Heat transfer enhancement through control of thermal dispersion effects, Int. J. Heat Mass Transfer 48 (2005) 2172.
[8] J.A. Eastman, S.U.S. Choi, S. Li, L.J. Thompson, S. Lee, Enhanced thermal conductivity through the development of nanofluids, in: 1996 Fall Meeting of the Materials Research Society (MRS), Boston, USA.
[9] J.A. Eastman, S.U.S. Choi, S. Li, W. Yu, L.J. Thompson, Anomalously increased effective thermal conductivities of ethylene glycol-based nanofluids containing copper nanoparticles, Appl. Phys. Lett. 78 (2001) 718–720.
[10] S.P. Jang, S.U.S. Choi, Role of Brownian motion in the enhanced thermal conductivity of nanofluids, Appl. Phys. Lett. 84 (2004) 4316–4318.
[11] S. Lee, S.U.S. Choi, Application of metallic nanoparticle suspensions in advanced cooling systems, in: 1996 International Mechanical Engineering Congress and Exhibition, Atlanta, USA.
[12] A. Ali, K. Vafai, A.-R.A. Khaled, Comparative study between parallel and counter flow configurations between air and falling film desiccant in the presence of nanoparticle suspensions, Int. J. Energy Res. 27 (2003) 725–745.
[13] N. Putra, W. Roetzel, S.K. Das, Natural convection of nanofluids, Heat Mass Transfer 39 (2003) 775–784.
[14] Y.M. Xuan, Q. Li, Heat transfer enhancement of nanofluids, Int. J. Heat Fluid Flow 21 (2000) 58–64.
[15] Y.M. Xuan, Q. Li, Investigation on convective heat transfer and flow features of nanofluids, ASME J. Heat Transfer 125 (2003) 151–155.
[16] B.C. Pak, Y.I. Cho, Hydrodynamic and heat transfer study of dispersed fluids with submicron metallic oxide particles, Exp. Heat Transfer 11 (1999) 151–170.
[17] Y. Yang, Z. Zhang, E. Grulke, W. Anderson, G. Wu, G. Heat, Transfer properties of nanoparticle-in-fluid dispersions (nanofluids) in laminar flow, Int. J. Heat Mass Transfer 48 (2005) 1107–1116.
[18] D.S. Wen, Y.L. Ding, Experimental investigation into the pool boiling heat transfer of aqueous based alumina nanofluids, J. Nanopart. Res. 7 (2005) 265–274.
[19] B.X. Wang, L.P. Zhou, X.F. Peng, A fractal model for predicting the effective thermal conductivity of liquid with suspension of nanoparticles, Int. J. Heat Mass transfer 46 (2003) 2665–2672.

[20] S.K. Das, N. Putra, W. Roetzel, Pool boiling characteristics of nanofluids, Int. J. Heat Mass transfer 46 (2003) 851–862.
[21] S.K. Das, N. Putra, W. Roetzel, Pool boiling of nanofluids on horizontal narrow tubes, Int. J. Multiphase Flow 29 (2003) 1237–1247.
[22] S.K. Das, N. Putra, P. Thiesen, W. Roetzel, Temperature dependence of thermal conductivity enhancement for nanofluids, J. Heat Transfer 125 (2003) 567–574.
[23] J. Kim, Y.T. Kang, C.K. Choi, Analysis of convective instability and heat transfer characteristics of nanofluids, Phys. Fluids 16 (2004) 2395–23401.
[24] A.G.A. Nanna, T. Fistrovich, K. Malinski, S.U.S. Choi, Thermal transport phenomena in buoyancy-driven nanofluids, in Proceedings of 2005 ASME International Mechanical Engineering Congress and RD&D Exposition, 15–17 November 2004, Anaheim, California, USA.
[25] A.G.A. Nnanna, M. Routhu, Transport phenomena in buoyancy-driven nanofluids – Part II, in: Proceedings of 2005 ASME Summer Heat Transfer Conference, 17–22 July 2005, San Francisco, California, USA.
[26] Y. Ding, H. Chen, L. Wang, et al., Heat transfer intensification using nanofluids, J. Particle Powder 25 (2007) 23–36.
[27] B.H. Chang, A.F. Mills, E. Hernandez, Natural convection of microparticle suspensions in thin enclosures, Int. J. Heat Mass Transfer 51 (2008) 1332–1341.
[28] C.J. Ho, W.K. Liu, Y.S. Chang, C.C. Lin, Natural convection heat transfer of alumina–water nanofluid in vertical square enclosures: an experimental study, Int. J. Therm. Sci. 49 (2010) 1345–1353.
[29] X. Wang, A. Mujumdar, Heat transfer characteristics of nanofluids: a review, Int. J. Therm. Sci. 46 (2007) 1–19.
[30] P. Keblinski, S.R. Phillpot, S.U.S. Choi, J.A. Eastman, Mechanisms of heat flow in suspensions of nano-sized particles (nanofluids, Int. J. Heat Mass Transfer 45 (2002) 855–863.
[31] J.A. Eastman, S.R. Phillpot, S.U.S. Choi, P. Keblinski, Thermal transport in nanofluids, Annu. Rev. Mater. Res. 34 (2004) 219–246.
[32] W. Evans, J. Fish, P. Keblinski, Role of Brownian motion hydrodynamics on nanofluid thermal conductivity, Appl. Phys. Lett. 88 (9) (2006) 93116.
[33] W. Yu, S.U.S. Choi, The role of interfacial layers in the enhanced thermal of nanofluids: a renovated Maxwell model, J. Nanopart. Res. 5 (1–2) (2003) 167–171.
[34] W. Yu, S.U.S. Choi, The role of interfacial layers in the enhanced thermal conductivity of nanofluids: a renovated Hamilton–Crosser model, J. Nanopart. Res. 6 (4) (2004) 355–361.
[35] Q. Xue, W.M. Xu, A model of thermal conductivity of nanofluids with interfacial shells, Mater. Chem. Phys. 90 (2005) 298–301.
[36] Q. Xue, Model for effective thermal conductivity of nanofluids, Phys. Lett. A 307 (2003) 313–317.
[37] H. Xie, M. Fujii, X. Zhang, Effect of interfacial nanolayer on the effective thermal conductivity of nanoparticle–fluid mixture, Int. J. Heat Mass Transfer 48 (2005) 2926–2932.
[38] L. Xue, P. Keblinski, S.R. Phillpot, S.U.S. Choi, J.A. Eastman, Effect of liquid layering at the liquid–solid interface on thermal transport, Int. J. Heat Mass Transfer 47 (19–20) (2004) 4277–4284.
[39] S.P. Jang, S.U. Choi, Free convection in a rectangular cavity (Benard convection) with nanofluids, in: Proceedings of the 2004 ASME International Mechanical Engineering Congress and Exposition, Anaheim, California, November 13–20, 2004.
[40] L. Gosselin, A.K. da Silva, Combined heat transfer and power dissipation optimization of nanofluid flows, Appl. Phys. Lett. 85 (2004) 4160.
[41] J. Lee, I. Mudawar, Assessment of the effectiveness of nanofluids for single-phase and two-phase heat transfer in micro-channels, Int. J. Heat Mass Transfer 50 (2007) 452–463.
[42] S.Q. Zhou, R. Ni, Measurement of the specific heat capacity of water-based Al_2O_3 nanofluid, Appl. Phys. Lett. 92 (2008) 093123.
[43] K.S. Hwang, J.H. Lee, S.P. Jang, Buoyancy-driven heat transfer of water-based Al_2O_3 nanofluids in a rectangular cavity, Int. J. Heat Mass Transfer 50 (2007) 4003–4010.
[44] C.J. Ho, M.W. Chen, Z.W. Li, Numerical simulation of natural convection of nanofluid in a square enclosure: effects due to uncertainties of viscosity and thermal conductivity, Int. J. Heat Mass Transfer 51 (2008) 4506–4516.
[45] A. Einstein, Eine neue bestimmung der molekuldimensionen, Ann. Phys., Leipzig 19 (1906) 289–306.
[46] H.C. Brinkman, The viscosity of concentrated suspensions and solutions, J. Chem. Phys. 20 (1952) 571.
[47] G. Batchelor, The effect of Brownian motion on the bulk stress in a suspension of spherical particles, J. Fluid Mech. 83 (1977) 97–117.
[48] T. Lundgren, Slow flow through stationary random beds and suspensions of spheres, J. Fluid Mech. 51 (1972) 273–299.
[49] A.L. Graham, On the viscosity of suspensions of solid spheres, Appl. Sci. Res. 37 (1981) 275–286.
[50] R.A. Simha, Treatment of the viscosity of concentrated suspensions, J. Appl. Phys. 23 (1952) 1020–1024.
[51] M. Mooney, The viscosity of a concentrated suspension of spherical particles, J. Colloid Sci. 6 (1951) 162–170.
[52] V.H. Eilers, Die viskocitat von emulsionen hochviskoser stoffe als funktion der konzentration, Kolloid-Zeitschrift 97 (1941) 313–321.
[53] N. Saito, Concentration dependence of the viscosity of high polymer solutions, J. Phys. Soc. Jpn. 5 (1950) 4–8.
[54] N.A. Frankel, A. Acrivos, On the viscosity of a concentrate suspension of solid spheres, Chem. Eng. Sci. 22 (1967) 847–853.
[55] X. Wang, X. Xu, S.U.S. Choi, Thermal conductivity of nanoparticles–fluid mixture, J. Thermophys. Heat Transfer 13 (1999) 474–480.
[56] H. Masuda, A. Ebata, K. Teramae, N. Hishinuma, Alteration of thermal conductivity and viscosity of liquid by dispersing ultra-fine particles (dispersion of c-Al_2 O_3, SiO_2 and TiO_2 ultra-fine particles), Netsu Bussei 4 (1993) 227–233.
[57] S. Maiga, S.J. Palm, C.T. Nguyen, G. Roy, N. Galanis, Heat transfer enhancement by using nanofluids in forced convection flows, Int. J. Heat Fluid Flow 26 (2005) 530–546.
[58] S. Maiga, C.T. Nguyen, N. Galanis, G. Roy, T. Mar'e, M. Coqueux, Heat transfer enhancement in turbulent tube flow using Al_2O_3 nanoparticle suspension, in: R.W. Lewis (Ed.), Int. J. Num. Meth. Heat Fluid Flow, vol. 16, 2006, pp. 275–292.
[59] P.K. Namburua, D.P. Kulkarni, D. Misra, D.K. Das, Viscosity of copper oxide nanoparticles dispersed in ethylene glycol and water mixture, Exp. Therm. Fluid Sci. 32 (2007) 397–402.
[60] C.T. Nguyen, F. Desgranges, G. Roy, N. Galanis, T. Maŕe, S. Boucher, H.A. Mintsa, Temperature and particle-size dependent viscosity data for water-based nanofluids–hysteresis phenomenon, Int. J. Heat Fluid Flow 28 (2007) 1492–1506.
[61] W.J. Tseng, K.C. Lin, Rheology and colloidal structure of aqueous TiO_2 nanoparticle suspensions, Mater. Sci. Eng. A355 (2003) 186–192.
[62] D.P. Kulkarni, D.K. Das, S.L. Patil, Effect of temperature on rheological properties of copper oxide nanoparticles dispersed in propylene glycol and water mixture, J. Nanosci. Nanotechnol. 7 (2007) 2318–2322.
[63] D.P. Kulkarni, D.K. Das, G. Chukwa, Temperature dependent rheological of copper oxide nanoparticles suspension (nanofluid), J. Nanosci. Nanotechnol. 6 (2006) 1150–1154.
[64] S.M.S. Murshed, K.C. Leong, C. Yang, Investigations of thermal conductivity and viscosity of nanofluids, Int. J. Therm. Sci. 47 (2008) 560–568.
[65] K.B. Anoop, S. Kabelac, T. Sundararajan, S.K. Das, Rheological and flow characteristics of nanofluids: influence of electroviscous effects and particle agglomeration, J. Appl. Phys. 106 (2009) 034909.
[66] H. Chen, Y. Ding, Y. He, Ch. Tan, Rheological behavior of ethylene glycol based titania nanofluids, Chem. Phys. Lett. 444 (2007) 333–337.
[67] J. Buongiorno, Convective transport in nanofluids, ASME J. Heat Transfer 128 (2006) 240–250.
[68] S.J. Palm, G. Roy, C.T. Nguyen, Heat transfer enhancement with the use of nanofluids in radial flow cooling systems considering temperature-dependent properties, Appl. Therm. Eng. 26 (2006) 2209–2218.
[69] W. Duangthongsuk, S. Wongwises, Measurement of temperature-dependent thermal conductivity and viscosity of TiO_2–water nanofluids, Exp. Therm. Fluid Sci. 33 (2009) 706–714.
[70] P.K. Namburu, D.K. Das, K.M. Tanguturi, R.S. Vajjha, Numerical study of turbulent flow and heat transfer characteristics of nanofluids considering variable properties, Int. J. Therm. Sci. 48 (2009) 290–302.
[71] P.K. Namburu, D.P. Kulkarni, D. Misra, D.K. Das, Viscosity of copper oxide nanoparticles dispersed in ethyleneglycol and water mixture, Exp. Therm. Fluid Sci. 32 (2007) 397–402.
[72] J. Koo, C. Kleinstreuer, Laminar nanofluid flow in microheat-sinks, Int. J. Heat Mass Transfer 48 (2005) 2652–2661.
[73] R.L. Hamilton, O.K. Crosser, Thermal conductivity of heterogeneous two-component systems, I&EC Fundam. 1 (1962) 182–191.
[74] J.C.A. Maxwell, Treatise on Electricity and Magnetism, second ed., Clarendon Press, Oxford, UK, 1881.
[75] D.A.G. Bruggeman, Berechnung verschiedener physikalischer konstanten von heterogenen substanzen, I. Dielektrizitatskonstanten und leitfahigkeiten der mischkorper aus isotropen substanzen, Ann. Phys., Leipzig, 24 (1935) 636–679.
[76] F.J. Wasp, Solid–Liquid Slurry Pipeline Transportation, Trans. Tech., Berlin, 1977.
[77] D.J. Jeffrey, Conduction through a random suspension of spheres, Proc. Roy. Soc. (Lond.) A335 (1973) 355–367.
[78] R.H. Davis, The effective thermal conductivity of a composite material with spherical inclusions, Int. J. Thermophys. 7 (1986) 609–620.
[79] S. Lu, H. Lin, Effective conductivity of composites containing aligned spherical inclusions of finite conductivity, J. Appl. Phys. 79 (1996) 6761–6769.
[80] Y. Xuan, Q. Li, W. Hu, Aggregation structure and thermal conductivity of nanofluids, AIChE J. 49 (4) (2003) 1038–1043.
[81] R. Prasher, P. Bhattacharya, P.E. Phelan, Thermal conductivity of nanoscale colloidal solutions (nanofluids), Phys. Rev. Lett. 94 (2) (2005) 025901.
[82] J. Koo, C. Kleinstreuer, A new thermal conductivity model for nanofluids, J. Nanopart. Res. 6 (6) (2004) 577–588.
[83] C.H. Chon, K.D. Kihm, S.P. Lee, S.U.S. Choi, Empirical correlation finding the role of temperature and particle size for nanofluid (Al_2O_3) thermal conductivity enhancement, Appl. Phys. Lett. 87 (2005) 153107.
[84] J. Lee, P.E. Gharago.zloo, B. Kolade, J.K. Eaton, K.E. Goodson, Nanofluid convection in microtubes, ASME J. Heat Transfer 132 (2010) 354–360.
[85] S. Lee, S.U.S. Choi, S. Li, J.A. Eastman, Measuring thermal conductivity of fluids containing oxide nanoparticles, ASME J. Heat Transfer 121 (1999) 280–289.
[86] C.H. Li, G.P. Peterson, The effect of particle size on the effective thermal conductivity of Al_2O_3–water nanofluids, J. Appl. Phys. 101 (2007) 044312.
[87] X. Zhang, H. Gu, M. Fujii, Effective thermal conductivity and thermal diffusivity of nanofluids containing spherical and cylindrical nanoparticles, J. Appl. Phys. 100 (2006) 1–5.

[88] E.V. Timofeeva, A.N. Gavrilov, J.M. McCloskey, Y.V. Tolmachev, Thermal conductivity and particle agglomeration in alumina nanofluids: experiment and theory, Phys. Rev. E 76 (2007) 061203.
[89] H.A. Minsta, G. Roy, C.T. Nguyen, D. Doucet, New temperature dependent thermal conductivity data for water-based nanofluids, Int. J. Therm. Sci. 48 (2009) 363–371.
[90] G. Roy, C.T. Nguyen, P.-R. Lajoie, Numerical investigation of laminar flow and heat transfer in a radial flow cooling system with the use of nanofluids, Superlatt. Microstruct. 35 (2004) 497–511.
[91] L.S. Sundar, K.V. Sharma, Experimental determination of thermal conductivity of fluid containing oxide nanoparticles, Int. J. Dynam. Fluids 4 (2008) 57–69.
[92] M. Golubovic, H.D.M. Hettiarachchi, W.M. Worek, W.J. Minkowycz, Nanofluids and critical heat flux, experimental and analytical study, Appl. Therm. Eng. 29 (2009) 1281–1288.
[93] H.S. Xue, J.R. Fan, R.H. Hong, Y.C. Hu, Characteristic boiling curve of carbon nanotube nanofluid as determined by the transient calorimeter technique, Appl. Phys. Lett. 90 (2007) 184107.
[94] H.D. Kim, J. Kim, et al., Experimental studies on CHF characteristics of nanofluids at pool boiling, Int. J. Multiphase Flow 33 (2007) 691–706.
[95] S.M. Murshed, S.H. Tan, N.T. Nguyen, Temperature dependence of interfacial properties and viscosity of nanofluids for droplet-based microfluidics, J. Phys. D: Appl. Phys. 41 (2008) 085502.
[96] D.S. Zhu, S.Y. Wu, N. Wang, Surface tension and viscosity of aluminum oxide nanofluids, in: The 6th International Symposium on Multiphase Flow, Heat Mass Transfer and Energy Conversion, AIP Conference Proceedings – March 1, 2010, vol. 1207, pp. 460–464.
[97] G. Prakash Narayan, K.B. Anoop, Sarit K. Das, Mechanism of enhancement/deterioration of boiling heat transfer using stable nanoparticle suspensions over vertical tubes, J. Appl. Phys. 102 (2007) 074317.
[98] S.M. You, J.H. Kim, K.H. Kim, Effect of nanoparticles on critical heat flux of water in pool boiling heat transfer, Appl. Phys. Lett. 83 (2003) 3374–3376.
[99] I.C. Bang, S.H. Chang, Boiling heat transfer performance and phenomena of Al_2O_3–water nanofluids from a plain surface in a pool, Int. J. Heat Mass Transfer 48 (2005) 2407–2419.
[100] J.P. Tu, N. Dinh, T. Theofanous, An experimental study of nanofluid boiling heat transfer, in: Proceedings of 6th International Symposium on Heat Transfer, Beijing, China, 2004.
[101] D.S. Wen, Y.L. Ding, Experimental investigation into the pool boiling heat transfer of aqueous based (-alumina nanofluids, J. Nanopart. Res. 7 (2005) 265–274.
[102] D.S. Wen, Y.L. Ding, R.A. Williams, Pool boiling heat transfer of aqueous based TiO_2 nanofluids, J. Enhanced Heat Transfer 13 (2006) 231–244.
[103] Z.H. Liu, J.G. Xiong, R. Bao, Boiling heat transfer characteristics of nanofluids in a flat heat pipe evaporator with micro-grooved heating surface, Int. J. Multiphase Flow 33 (2007) 1284–1295.
[104] M.H. Kim, J.B. Kim, H.D. Kim, Experimental studies on CHF characteristics of nano-fluids at pool boiling, Int. J. Multiphase Flow 33 (2007) 691–706.
[105] S.J. Kim, T. McKrell, J. Buongiorno, L.W. Hu, Experimental study of flow critical heat flux in alumina–water, zinc-oxide–water and diamond–water nanofluids, J. Heat Transfer 131 (4) (2009).
[106] P. Vassallo, R. Kumar, S.D. Amico, Pool boiling heat transfer experiments in silica–water nanofluids, Int. J. Heat Mass Transfer 47 (2004) 407–411.
[107] C.H. Li, B.X. Wang, X.F. Peng, Experimental investigations on boiling of nano-particle suspensions, in: 2003 Boiling Heat Transfer Conference, Jamica, USA.
[108] S.J. Kim, I.C. Bang, J. Buongiorno, L.W. Hu, Effects of nanoparticle deposition on surface wettability influencing boiling heat transfer in nanofluids, Appl. Phys. Lett. 89 (2006) 153107.
[109] S.J. Kim, I.C. Bang, J. Buongiorno, L.W. Hu, Surface wettability change during pool boiling of nanofluids and its effect on critical heat flux, Int. J. Heat Mass Transfer 50 (2007) 4105–4116.
[110] K. Sefiane, On the role of structural disjoining pressure and contact line pinning in critical heat flux enhancement during boiling of nanofluids, Appl. Phys. Lett. 89 (2006) 044106.
[111] R. Hegde, S.S. Rao, R.P. Reddy, Critical heat flux enhancement in pool boiling using alumina nanofluids, Heat Transfer, Heat Transfer—Asian Res. 39 (2010) 323–331.
[112] T.M. Anderson, I. Mudawar, Microelectronic cooling by enhanced pool boiling of a dielectric fluorocarbon liquid, ASME J. Heat Transfer 111 (1989) 752–759.
[113] I. Mudawar, T.M. Anderson, Optimization of enhanced surfaces for high flux chip cooling by pool boiling, ASME J. Electron. Packag. 115 (1993) 89–99.
[114] H. Honda, H. Takamastu, J.J. Wei, Enhanced boiling of FC-72 on silicon chips with micro-pin-fins and submicron-scale roughness, ASME J. Heat Transfer 124 (2002) 383–389.
[115] J.J. Wei, H. Honda, L.J. Guo, Experimental study of boiling phenomena and heat transfer performances of FC-72 over micro-pin-finned silicon chips, Heat Mass Transfer 41 (2005) 744–755.
[116] S. Ujereh, T. Fisher, I. Mudawar, Effects of carbon nanotube arrays on nucleate pool boiling, Int. J. Heat Mass Transfer 50 (2007) 4023–4038.